EVLA Memo No. 218
Radome Tests in Situ of Antenna ea11

Pedro P.B. Beaklini, Vivek Dhawan, Paul Demorest

May 16th 2022

ABSTRACT

In this memo, we will show the plots regarding the tests of the performance of the VLA antenna with a new radome (see EVLA Memo No. 213) . On Wednesday, April 13th, the new radome was installed in antenna ea11 in front of the horns of bands X, Ku, K, Ka, and Q. We have performed four observations of two bright sources before and after the changing of the radome to search for any signs of the radome change. We did not find any changes in the signal (Tsys, amplitude or phase) that could be attributed to the new radome material. All changes seen in ea11 between different days were also seen in other antennas, and they can be explained by wind, source elevation or weather.

1. Description

We chose two sources to do our analysis: 3C84 and 3C286. The first one is a strong unpolarized source, but with the disadvantage of being in the sky during the daytime in April, which can be challenging for the high frequencies in an epoch of strong winds. The second source, 3C286, is a flux calibrator with a known model rising at night but with the disadvantage of being a polarized source. After debating which source should be selected, we decided to observe both. The scheduling blocks have the following structures: after the setup and pointing scans, there are several short scans of 1 minute on the source. It was 8 scans at Q-band, 6 at Ka-band, 5 at K, Ku, and X-band. We added a tipping scan after each band to track eventual changes in Tsys with the elevation. We have used an 8-bit sampler with 16 spws with 64 channels of 2 MHz. We show the hardware setup in table 1.

Table 1: Hardware setup

Band	A0/C0 (GHz)	B0/D0 (GHz)
Q	44.50	45.50
Ka	32.52	31.52
K	23.00	24.00
Ku	14.50	13.50
X	9.50	10.50

2. Observations

We have performed 4 observations with the old radome, i.e., before the change, and 4 observations with the new radome material. Antenna ea11 was at the master pad, and we have used ea28 as a reference antenna and ea03, the closest by ea11, to check eventual changes. The observations of 3C84 occurred before the sunset, while the data obtained for 3C286 was acquired soon after sunset. The tipping scans were identified as night and day. We have pointed to the north direction in both cases, changing the azimuth to EAST/WEST to avoid large slew times. For 3C84 SB the tipping was performed at AZ 300 deg, while for 3C286 SB at AZ 80 deg. In table 2, we summarize our observation schedule. The files names on the data archive are in the appendix A.

Table 2: Summary of our observations. We will label each run by source & day (first column)

Source & Day	Date (2022)	Elevation (start-end) deg	Wind	API RMS (degs)	Radome material
3C84 day 1	April 9th	52-40	SE at 8.3 m/s	2.6	OLD
3C286 day 1*	April 9th	45-62	N at 2.0 m/s	5.1	OLD
3C84 day 2**	April 10th	60-48	SW at 13.4 m/s	7.9	OLD
3C286 day 2	April 10th	45-62	SW at 3.4 m/s	2.8	OLD
3C84 day 3**	April 15th	61-49	SW at 10 m/s	5.5	NEW
3C286 day 3	April 14th	30-44	W at 3.7 m/s	5.2	NEW
3C84 day 4	April 16th	47-35	SW at 10.6 m/s	4.3	NEW
3C286 day 4	April 15th	34-50	SW at 8.1 m/s	4.3	NEW

(*) Antenna ea11 not used for Ku, and X bands. So we partially lost this data set.
(**) Observation started before midnight UT, log date are on April 9th and on April 14th.

3. Results

Comparing the data with the old and the new radome material, we did not find significant changes in the data. Minor changes that were seen in ea11 were also seen in ea03, the closest one of the ea11. We show all plots in the following pages for a close look, where we average all data through time binned in 16 MHz.

We have organized the plot as follows: data obtained with the old radome are represented as filled dots, while data obtained with the new radome are indicated by crosses, different colors mean different days. We separated plots in right-hand and left-hand polarization; between the sources 3C84 and 3C286; and between the bands. Figures in section 4.1 show the bandpass calibration table computed in both amplitude and phase. In section 4.2, we show Tsys on source and in section 4.3 we show the Tsys in tipping curves. Finally, one last test is shown in section 4.4: to check for any non-expected cross-hand signature and to highlight eventual differences, we used the bandpass solution of the data obtained with the old radome and applied it to the data with the new radome. The idea is that even minor changes would be highlighted. This analise did not work well in the 3C84 observations at high frequency, observed during day-time, but any eventual changes we found were also presented in other antennas. For that source, we will show here only the X and the Ku-band plots.

4. Plots

4.1 Bandpass calibration tables

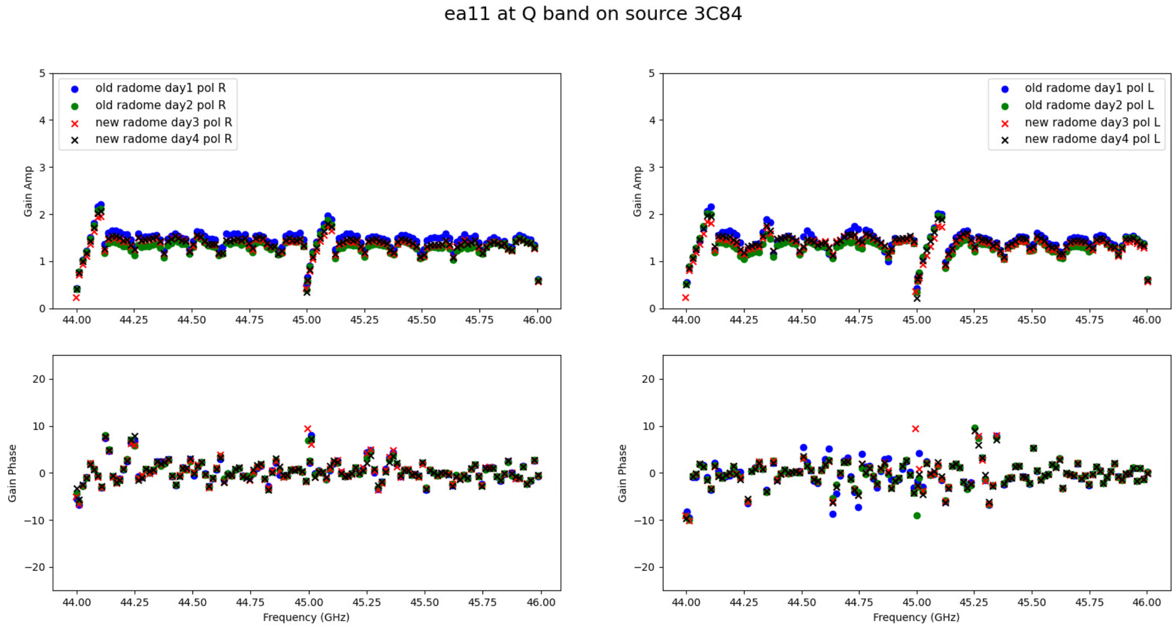

Figure 1: Bandpass calibration table for Q-band on 3C84 data with the old and new radome material. Changes between the days are seen, but are even higher between day 1 and day 2, both obtained with the old radome material. No changes that could be attributed to the new radome material was seen.

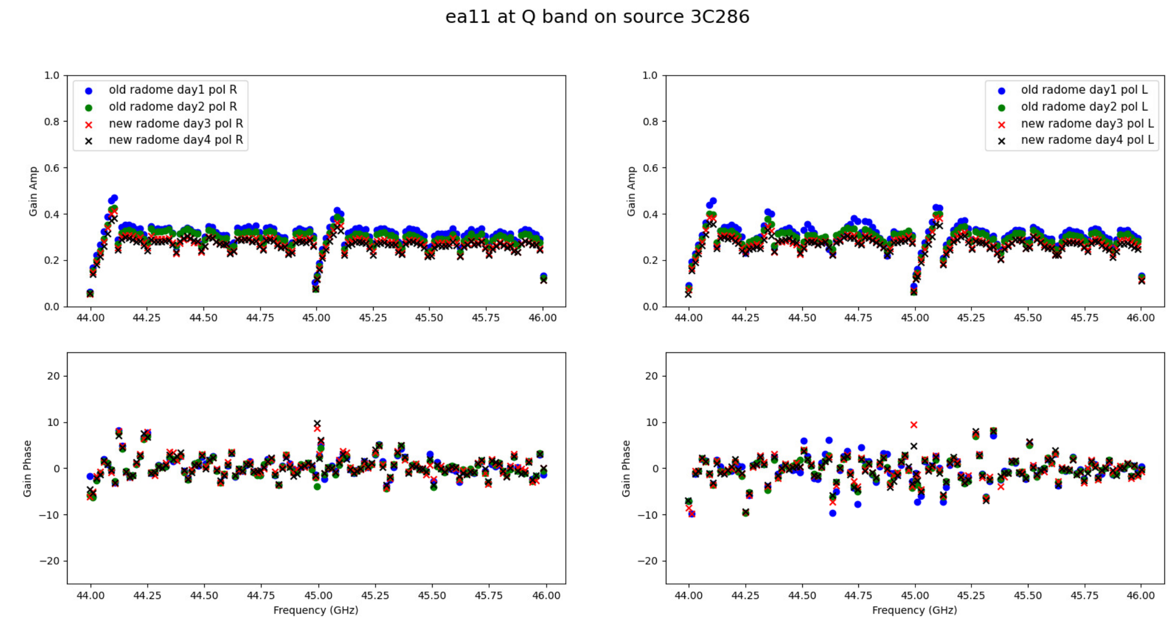

Figure 2: Bandpass calibration table for Q-band on 3C286 data with the old and new radome material. Changes between the days are seen, but are even higher between day 1 and day 2, both obtained with the old radome material. No changes that could be attributed to the new radome material was seen.

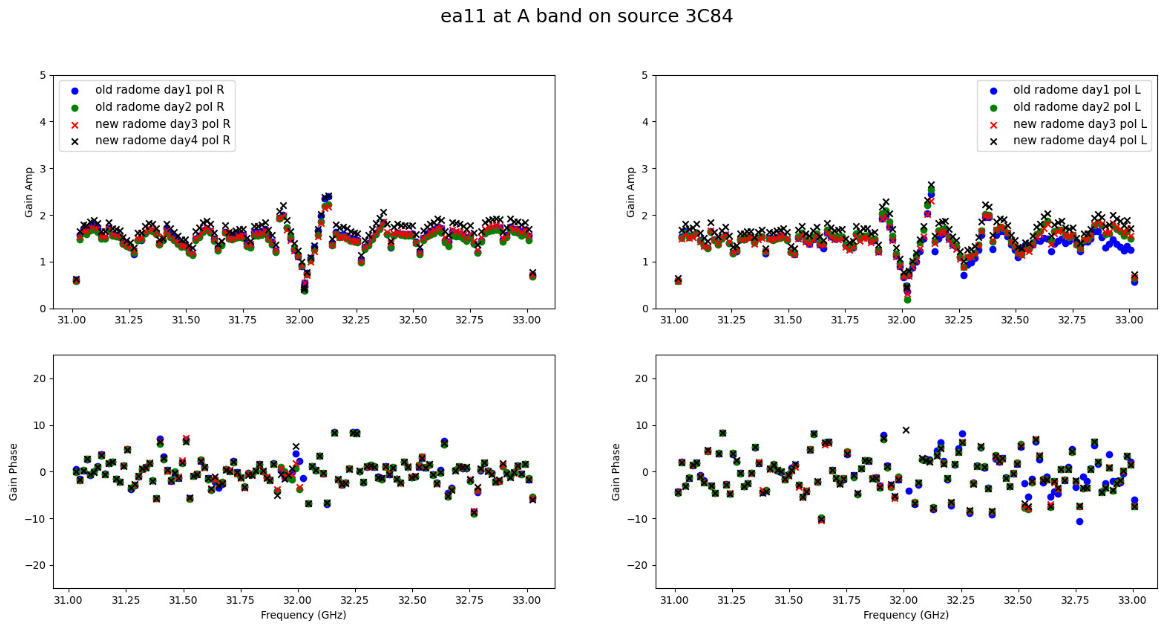

Figure 3: Bandpass calibration table for Ka-band on 3C84 data with the old and new radome material. We see a good match between the days. No changes that could be attributed to the new radome material was seen.

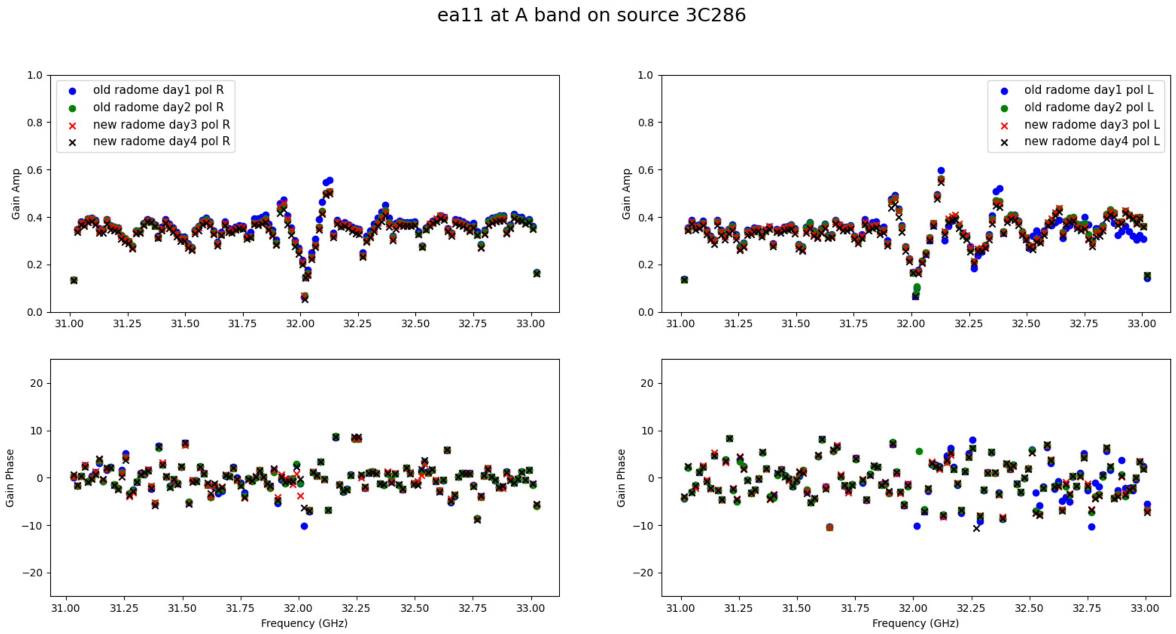

Figure 4: Bandpass calibration table for Ka-band on 3C286 data with the old and new radome material. We see a good match between the days. No changes that could be attributed to the new radome material was seen.

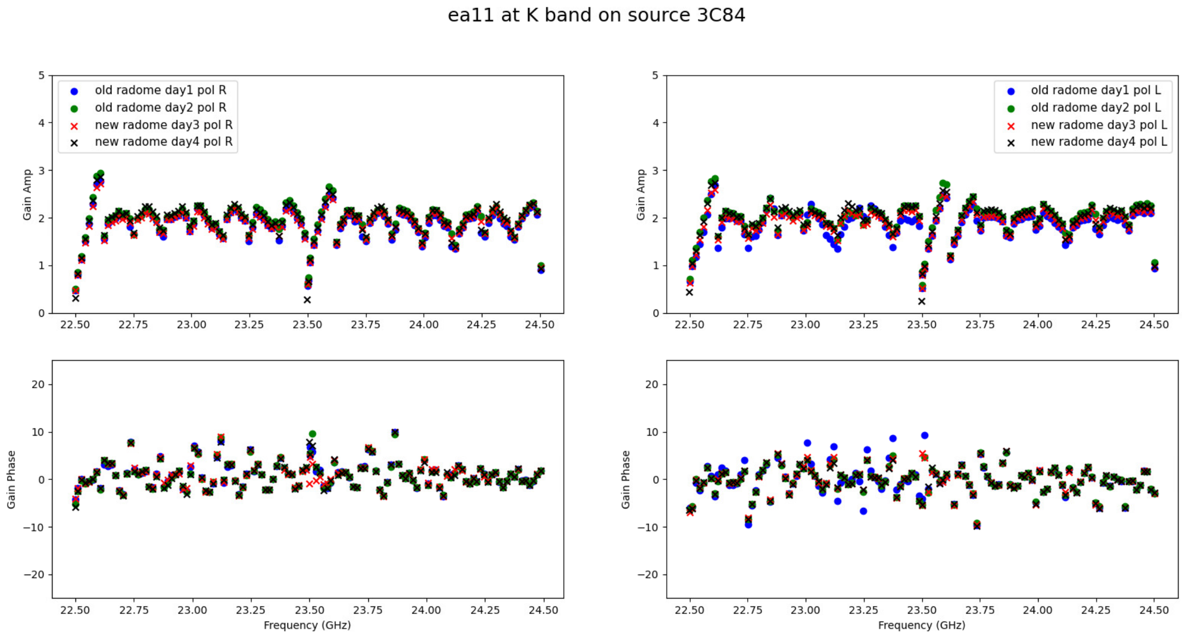

Figure 5: Bandpass calibration table for K-band on 3C84 data with the old and new radome material. Day 1 shows small differences, but day 3 and day 4 both match well with day 2. No changes that could be attributed to the new radome material was seen.

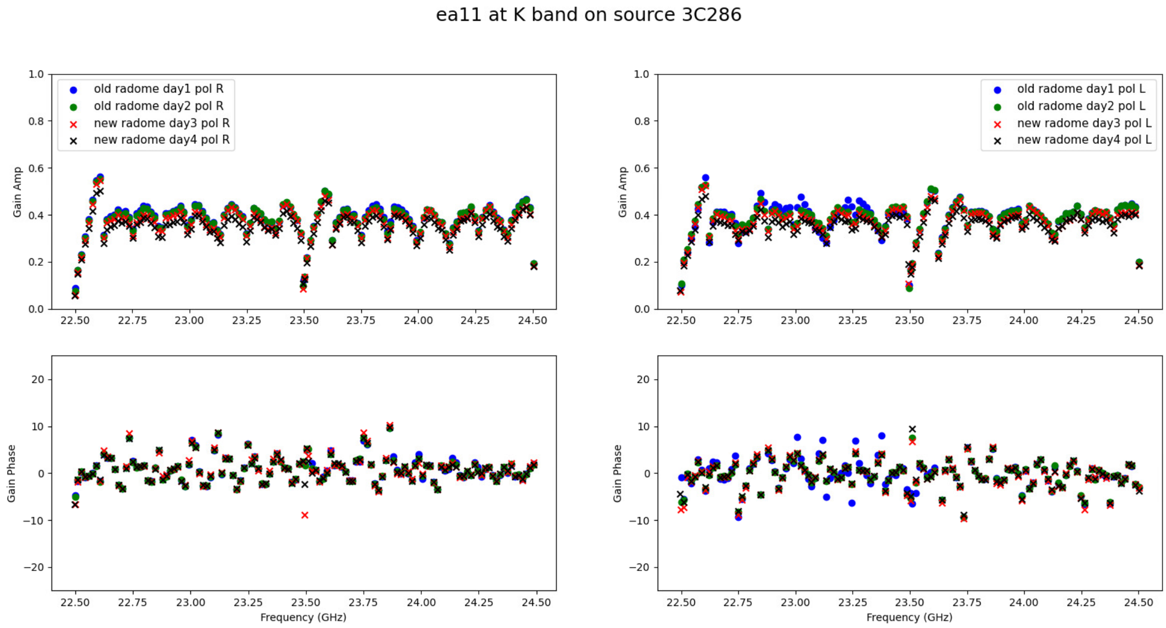

Figure 6: Bandpass calibration table for K-band on 3C286 data with the old and new radome material. Day 1 shows small differences, but day 3 and day 4 both match well with day 2. No changes that could be attributed to the new radome material was seen.

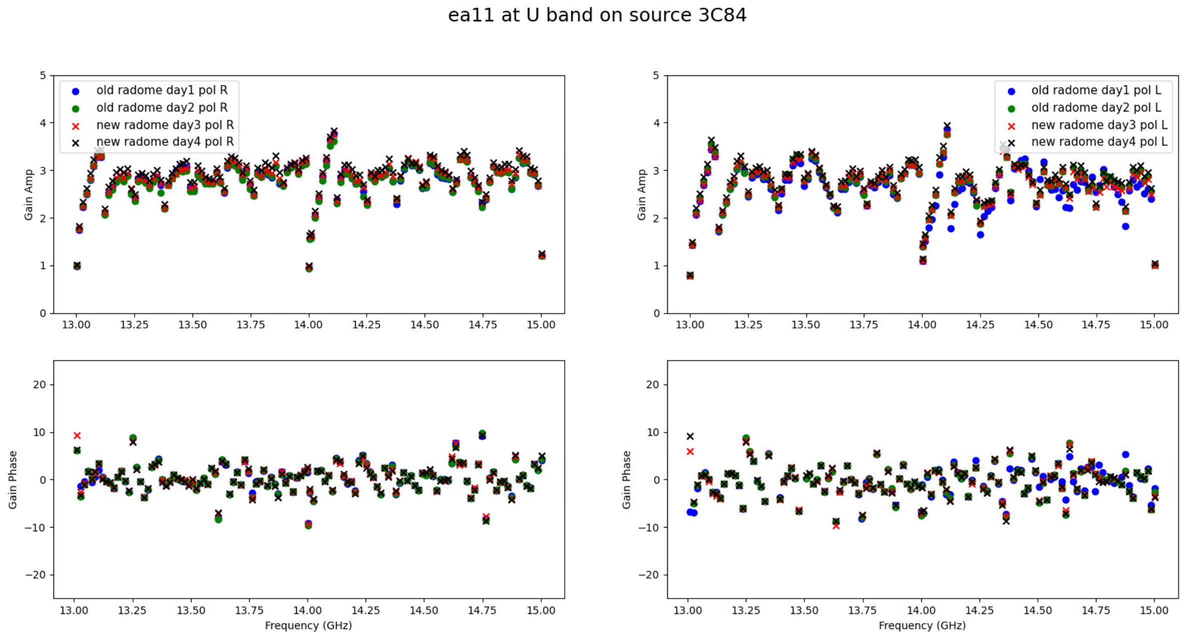

Figure 7: Bandpass calibration table for Ku-band on 3C84 data with the old and new radome material. Day 1 shows small differences, but day 3 and day 4 both match well with day 2. No changes that could be attributed to the new radome material was seen.

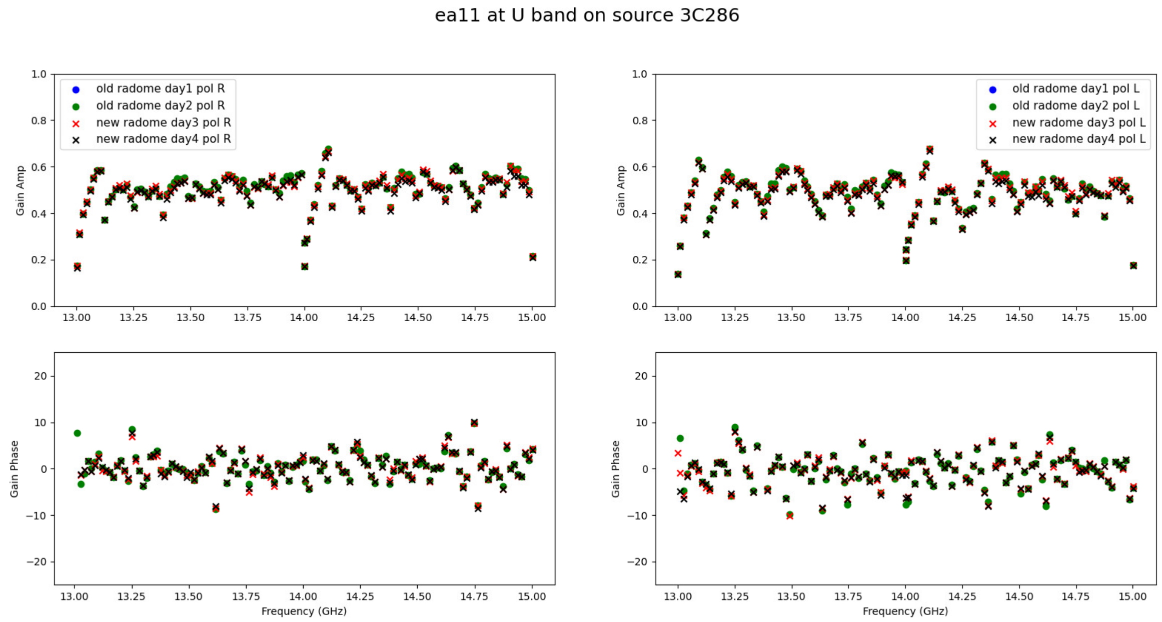

Figure 8: Bandpass calibration table for Ku-band on 3C84 data with the old and new radome material. We do not have day 1 (see comment on table 2), but day 3 and day 4 both match well with day 2. No changes that could be attributed to the new radome material was seen.

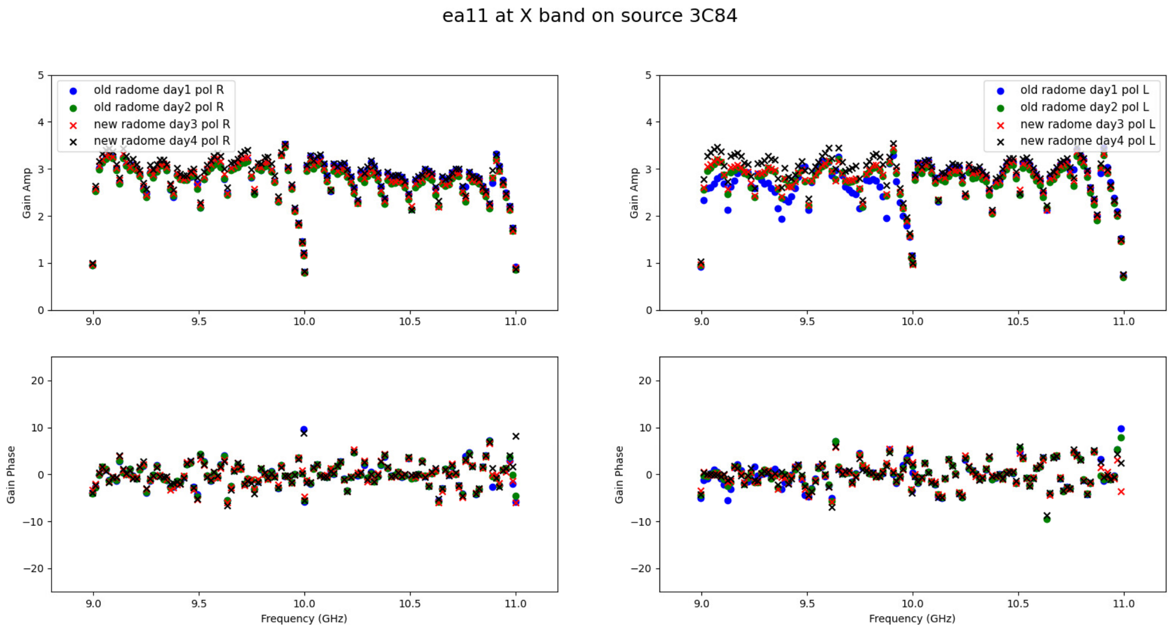

Figure 9: Bandpass calibration table for X-band on 3C84 data with the old and new radome material. Day 1 shows small differences on L, but day 3 and day 4 both match well with day 2. No changes that could be attributed to the new radome material was seen.

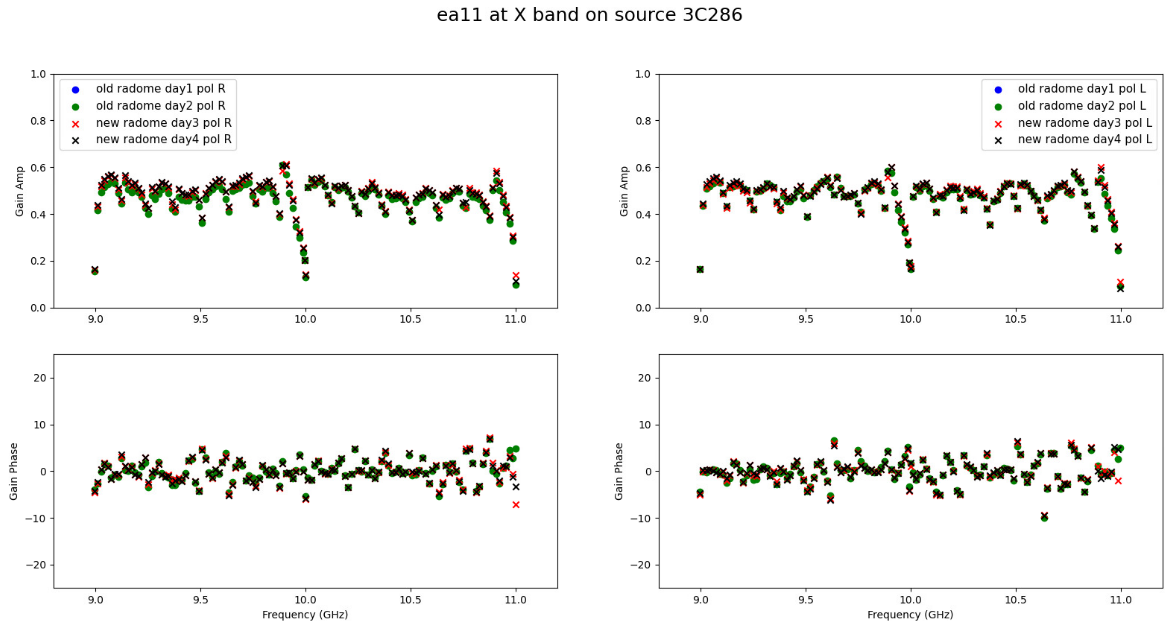

Figure 10: Bandpass calibration table for Ku-band on 3C286 data with the old and new radome material. We do not have day 1 (see comment on table 2), but day 3 and day 4 both match well with day 2. No changes that could be attributed to the new radome material was seen.

4.2 Tsys

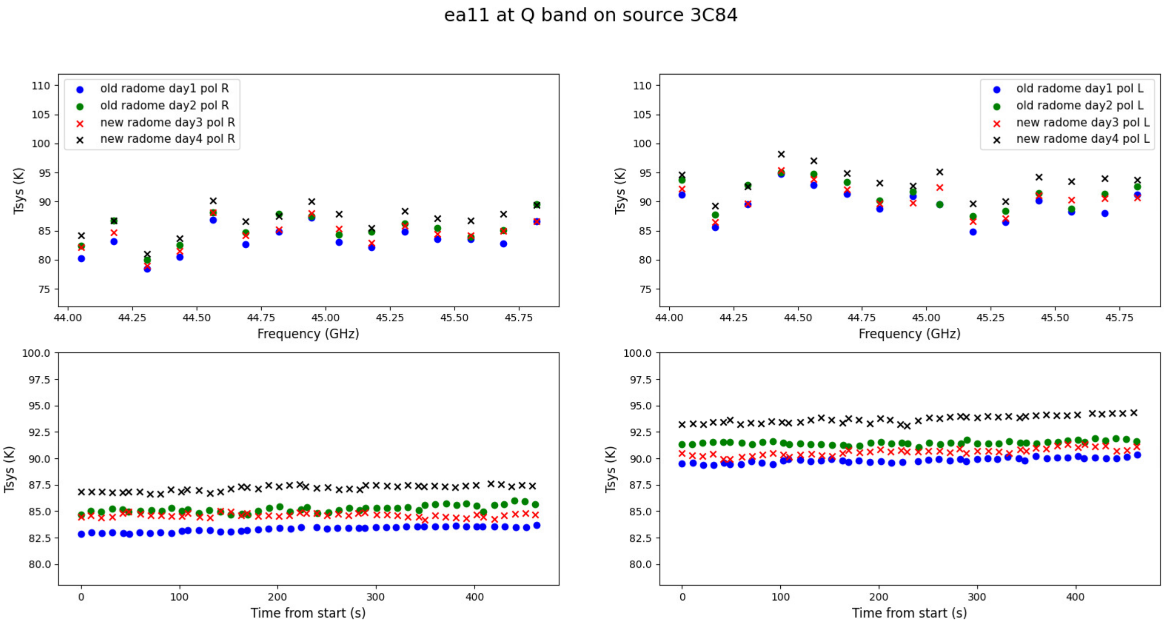

Figure 11: Tsys on source 3C84 at Q-band. It shows the same variability pattern between the days. We concluded that no differences could be attributed to the new radome material.

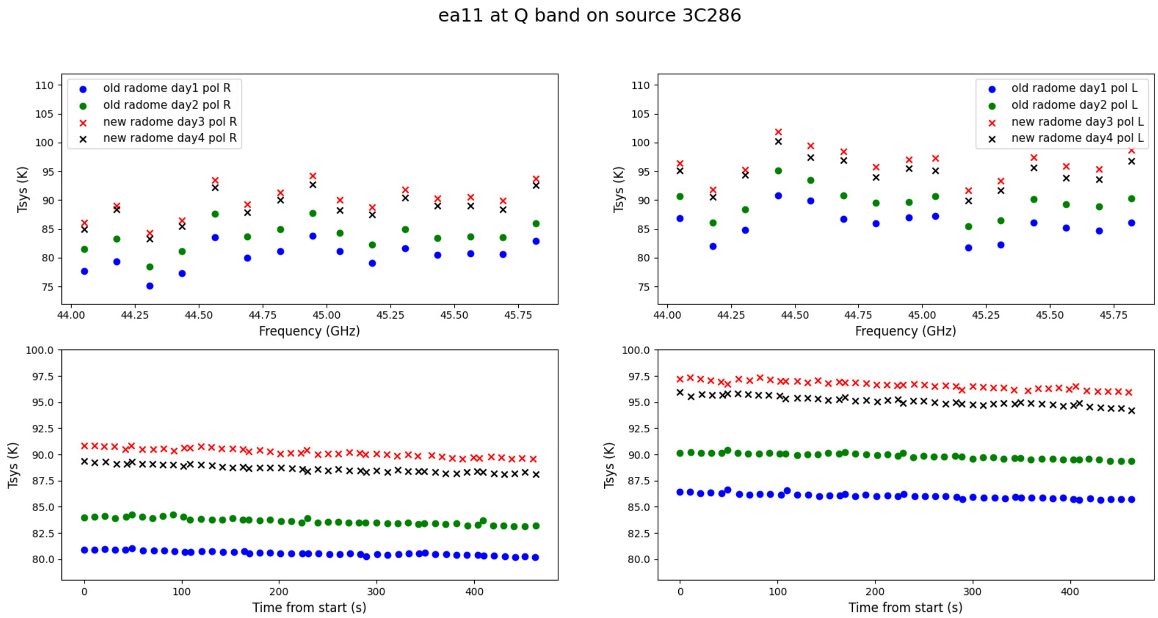

Figure 12: Tsys on source 3C286 at Q-band. Here we show significant changes in Tsys level due to the different elevation. This is seen in bands Q,Ka,K and Ku, but is also presented in antenna ea03(see figures 21 to 24, pages 13 and 14). We concluded that no differences could be attributed to the new radome material.

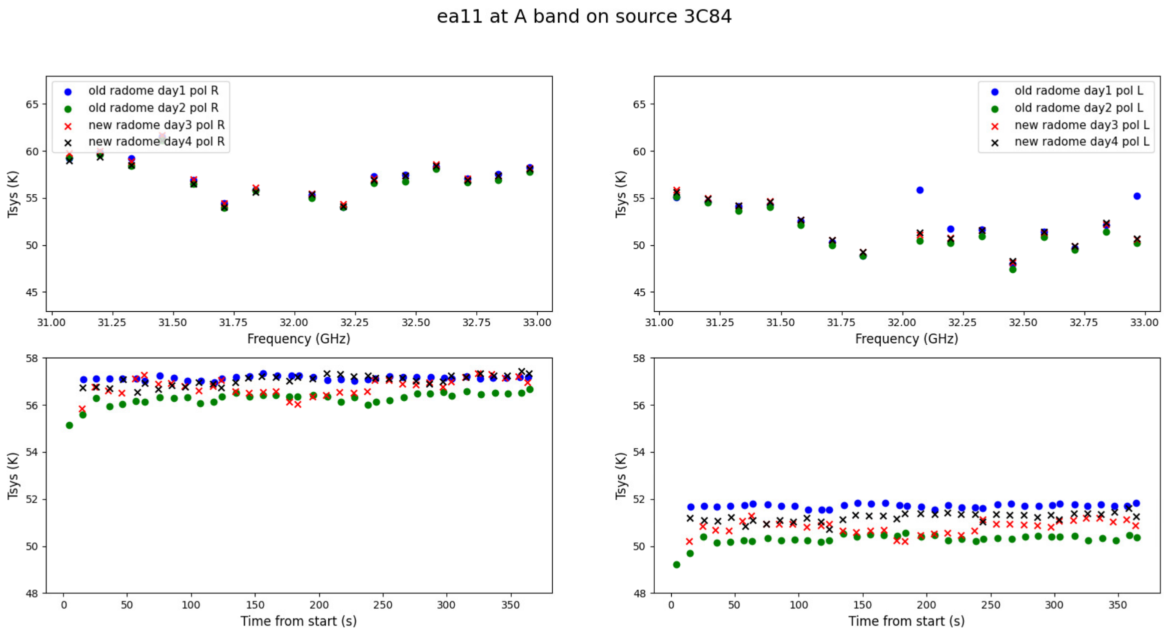

Figure 13: Tsys on source 3C84 at Ka-band. It shows the same variability pattern between the days. We concluded that no differences could be attributed to the new radome material.

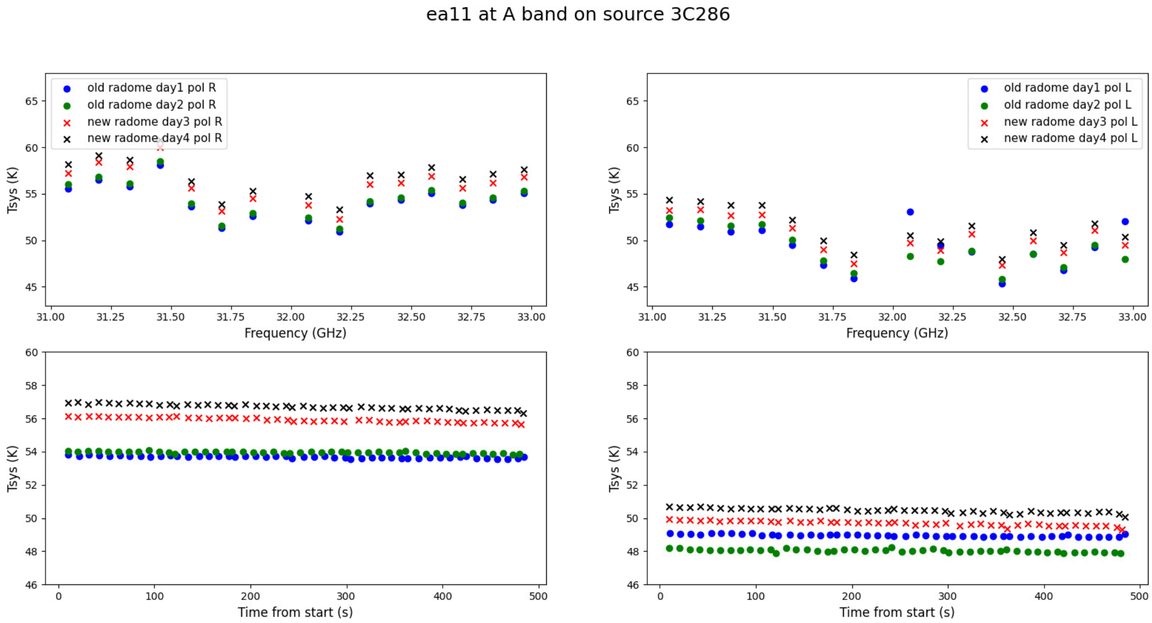

Figure 14: Tsys on source 3C286 at Ka-band.Here we show significant changes in Tsys level due to the different elevation. This is seen in bands Q,Ka,K and Ku, but is also presented in antenna ea03(see figures 21 to 24, pages 13 and 14). We concluded that no differences could be attributed to the new radome material.

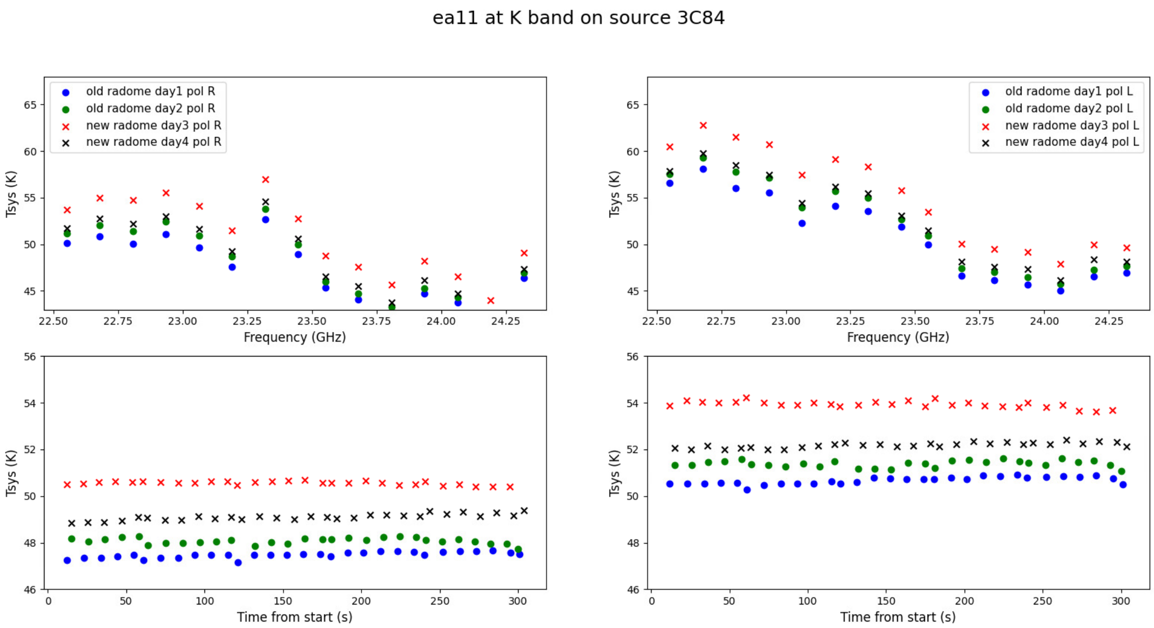

Figure 15: Tsys on source 3C84 at K-band. Here we show significant changes in Tsys level. However, similar differences were also seen in antennas ea03 and ea28 (Figure 25 and 26 on page 15). We concluded that no differences could be attributed to the new radome material.

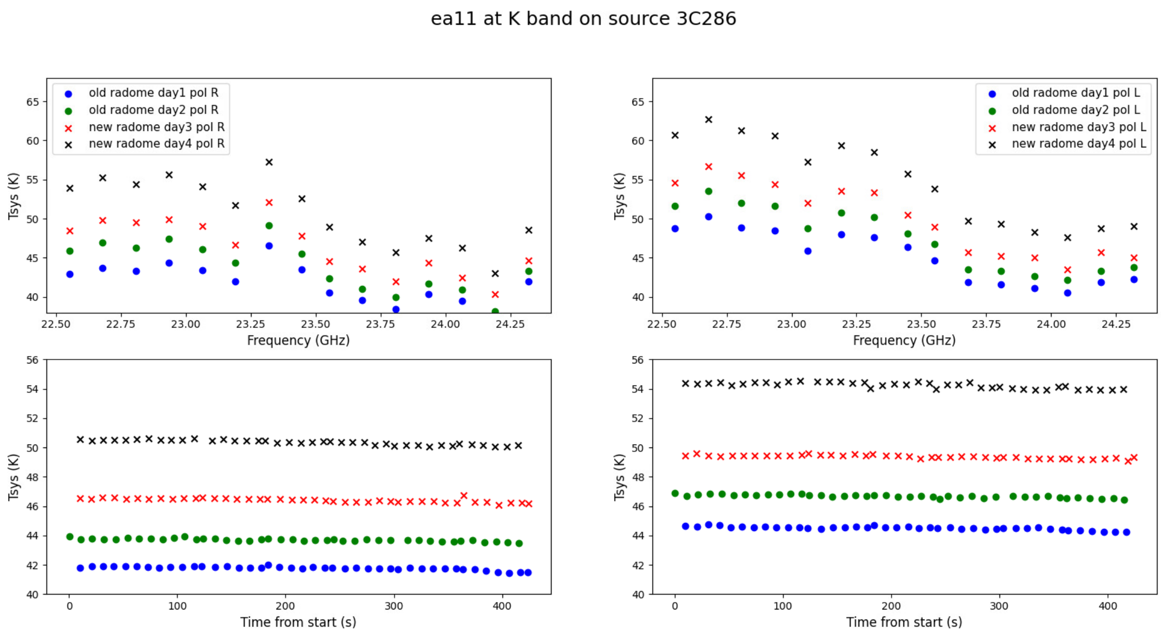

Figure 16: Tsys on source 3C286 at K-band. Here we show significant changes in Tsys level due to the different elevation. This is seen in bands Q,Ka,K and Ku, but is also presented in antenna ea03(see figures 21 to 24, pages 13 and 14). We concluded that no differences could be attributed to the new radome material.

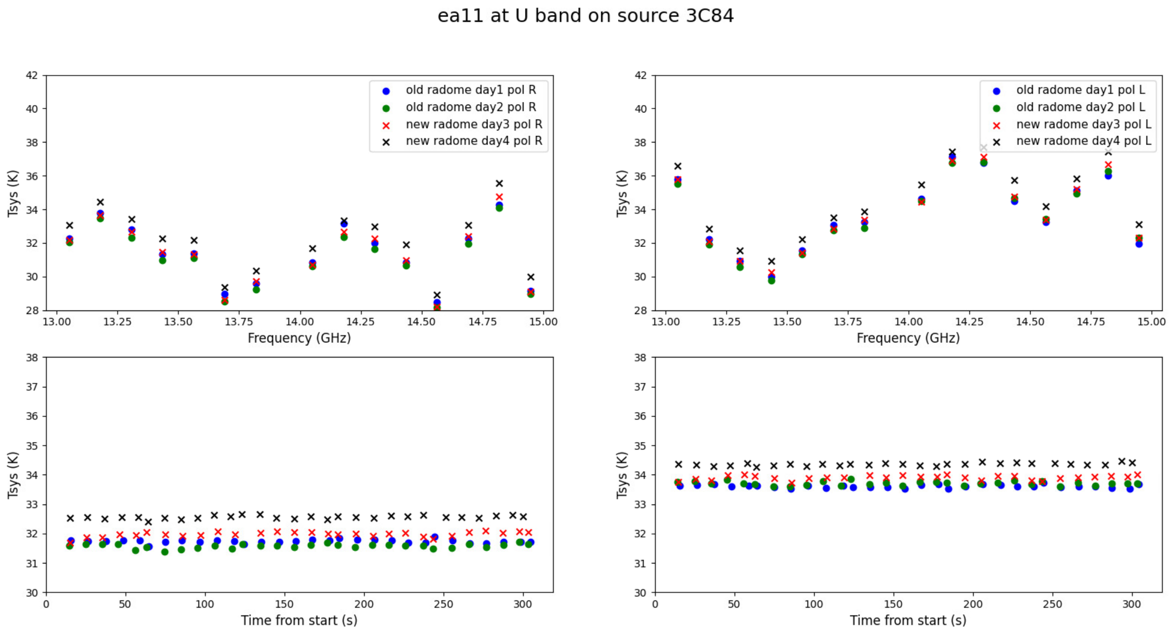

Figure 17: Tsys on source 3C84 at Ku-band. It shows the same variability pattern between the days. We concluded that no differences could be attributed to the new radome material.

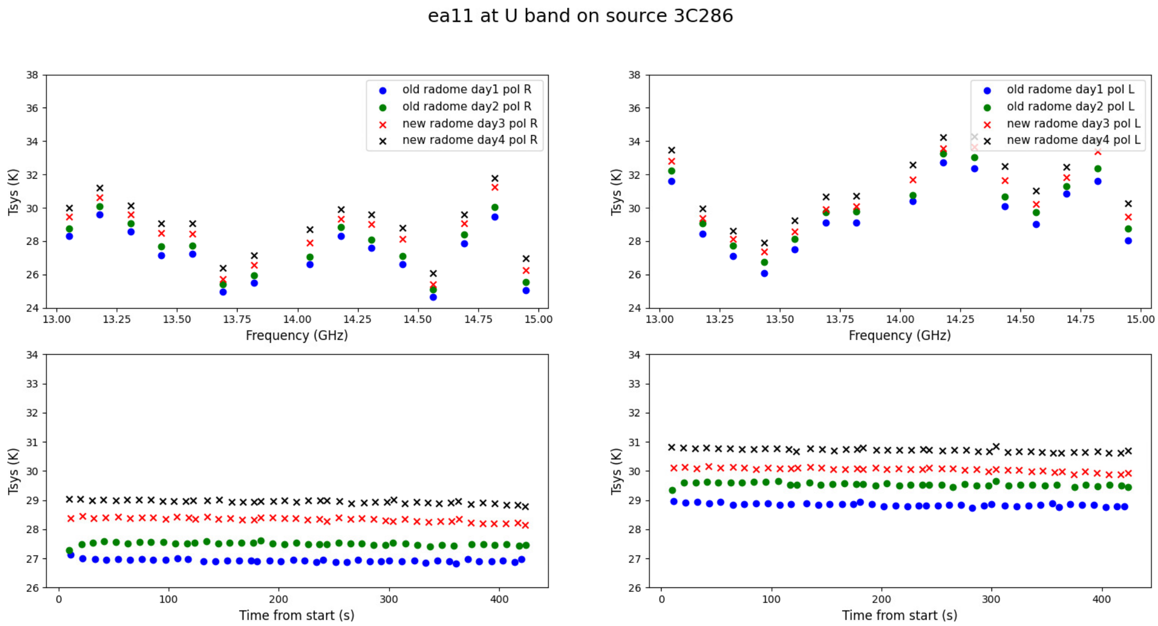

Figure 18: Tsys on source 3C286 at K-band. Here we show significant changes in Tsys level due to the different elevation. This is seen in bands Q,Ka,K and Ku, but is also presented in antenna ea03(see figures 21 to 24, pages 13 and 14). We concluded that no differences could be attributed to the new radome material.

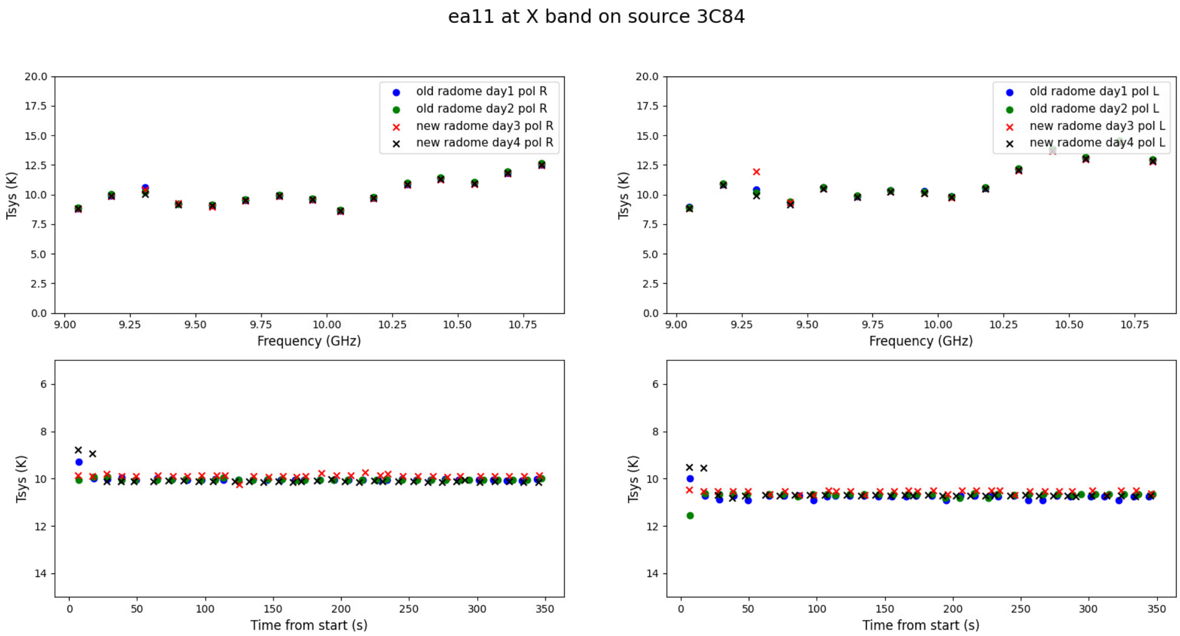

Figure 19: Tsys on source 3C84 at X-band. It shows the same variability pattern between the days. We concluded that no differences could be attributed to the new radome material.

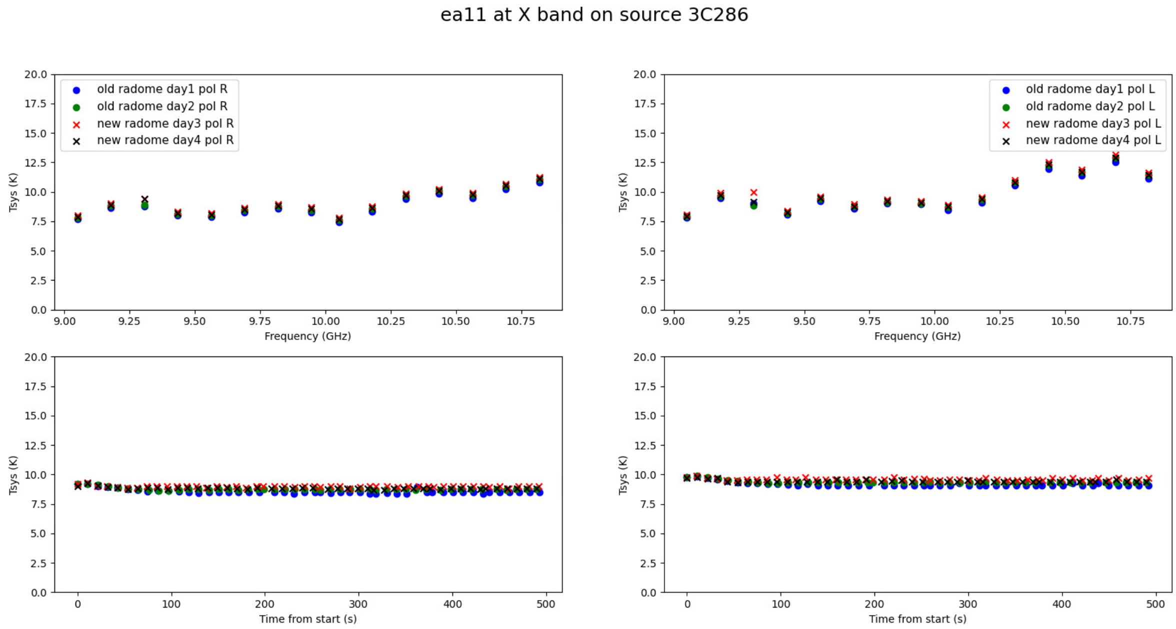

Figure 20: Tsys on source 3C84 at X-band. It shows the same variability pattern between the days. We concluded that no differences could be attributed to the new radome material.

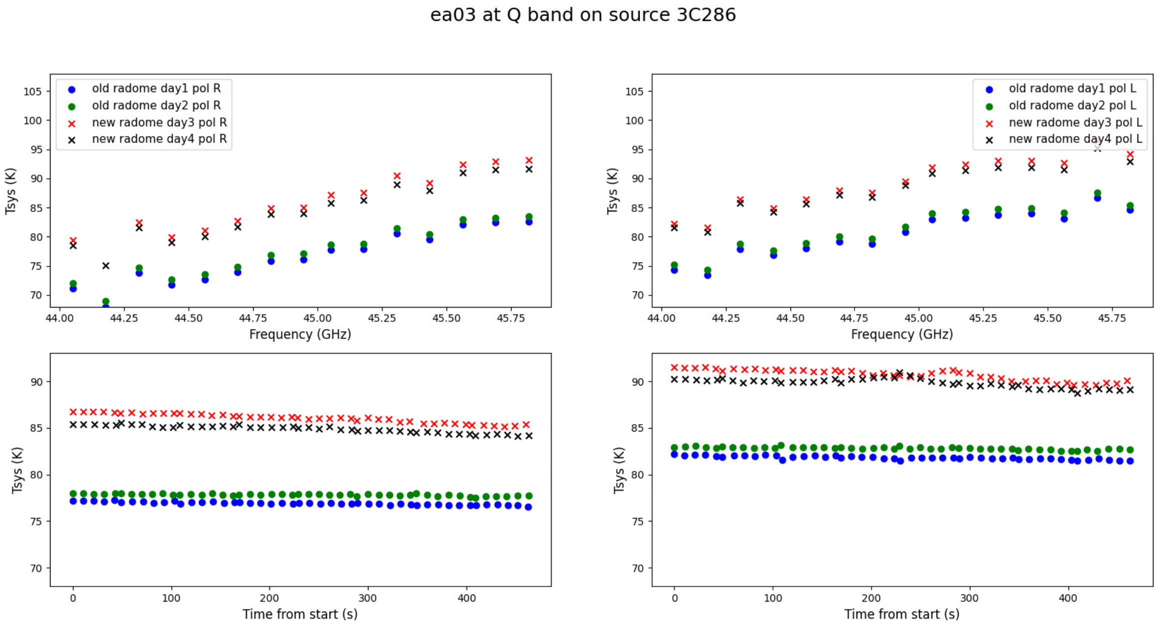

Figure 21: Same differences between the days seen in ea11 band Q (figure 12, page 8) in antenna ea03.

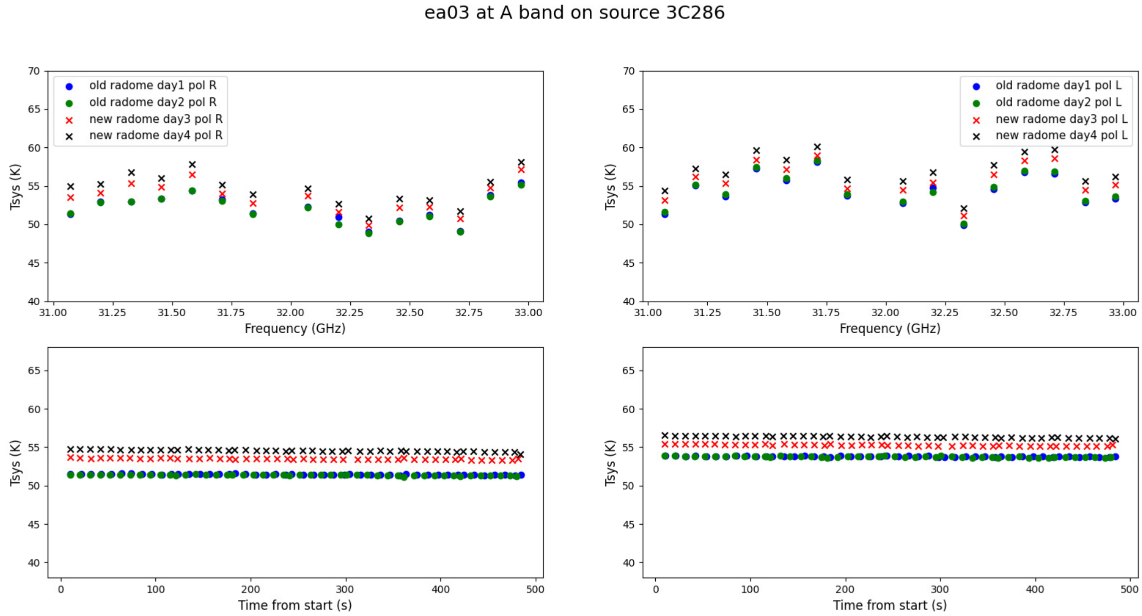

Figure 22: Same differences between the days seen in ea11 band Ka (figure 14, page 9) in antenna ea03.

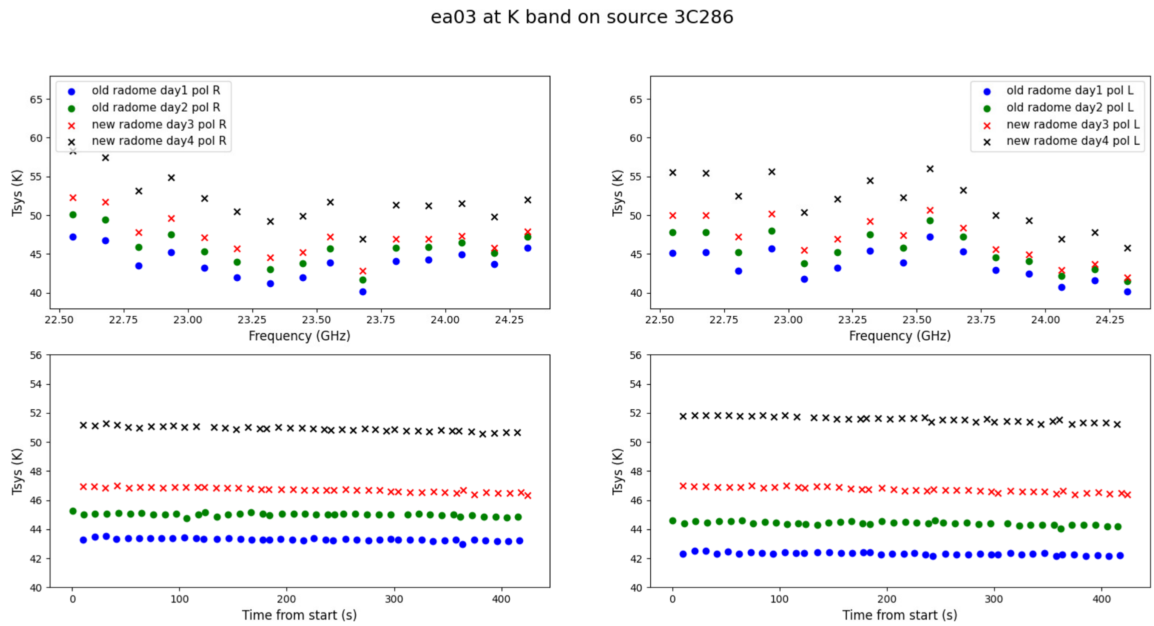

Figure 23: Same differences between the days seen in ea11 band K (figure 16, page 10) in antenna ea03.

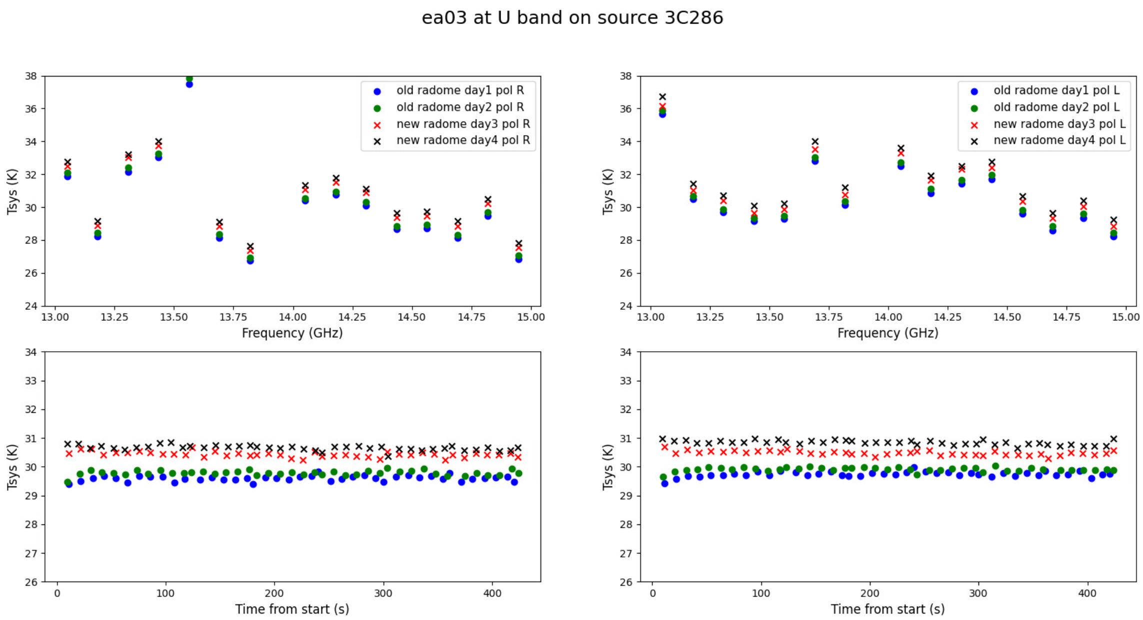

Figure 24: Same differences between the days seen in ea11 band Ku (figure 18, page 11) in antenna ea03.

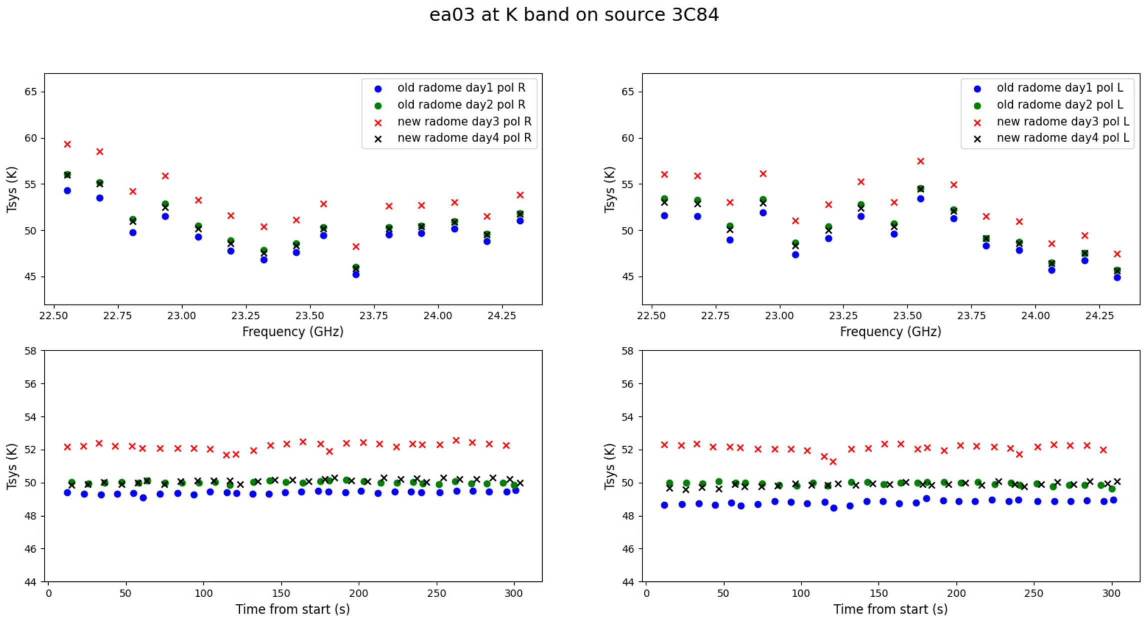

Figure 25: Differences in Tsys at K-band seen in ea11 (figure 15, page 10) was also seen in ea03 and ea28(Figure 26).

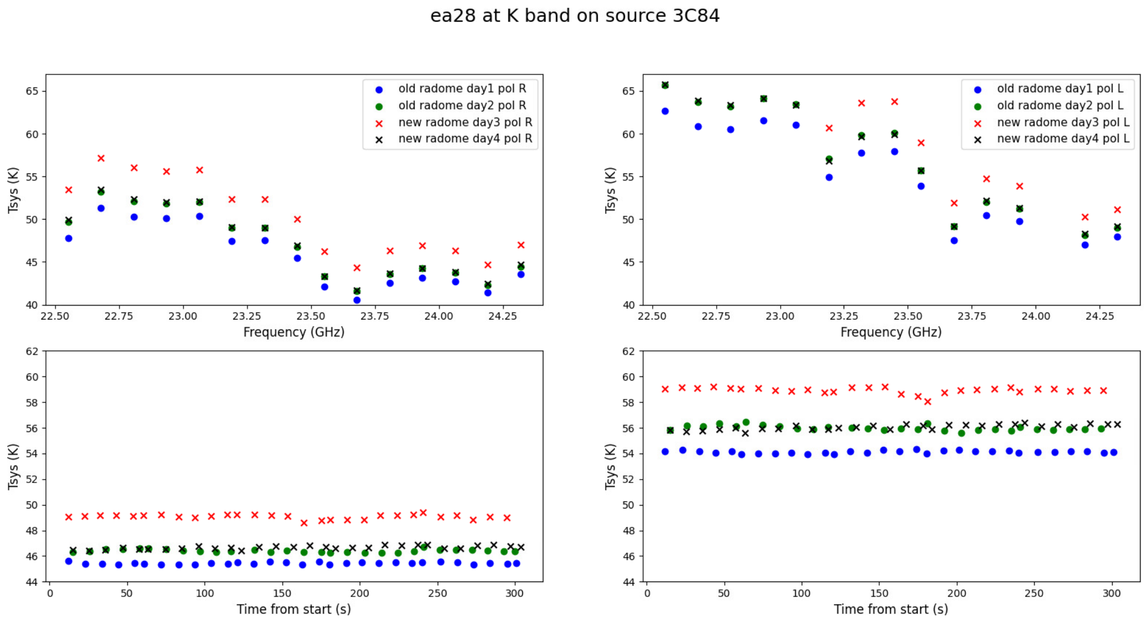

Figure 26: Differences in Tsys at K-band seen in ea11 (figure 15, page 10) was also seen in ea03 (Figure 25) and ea28.

4.3 Tipping curves

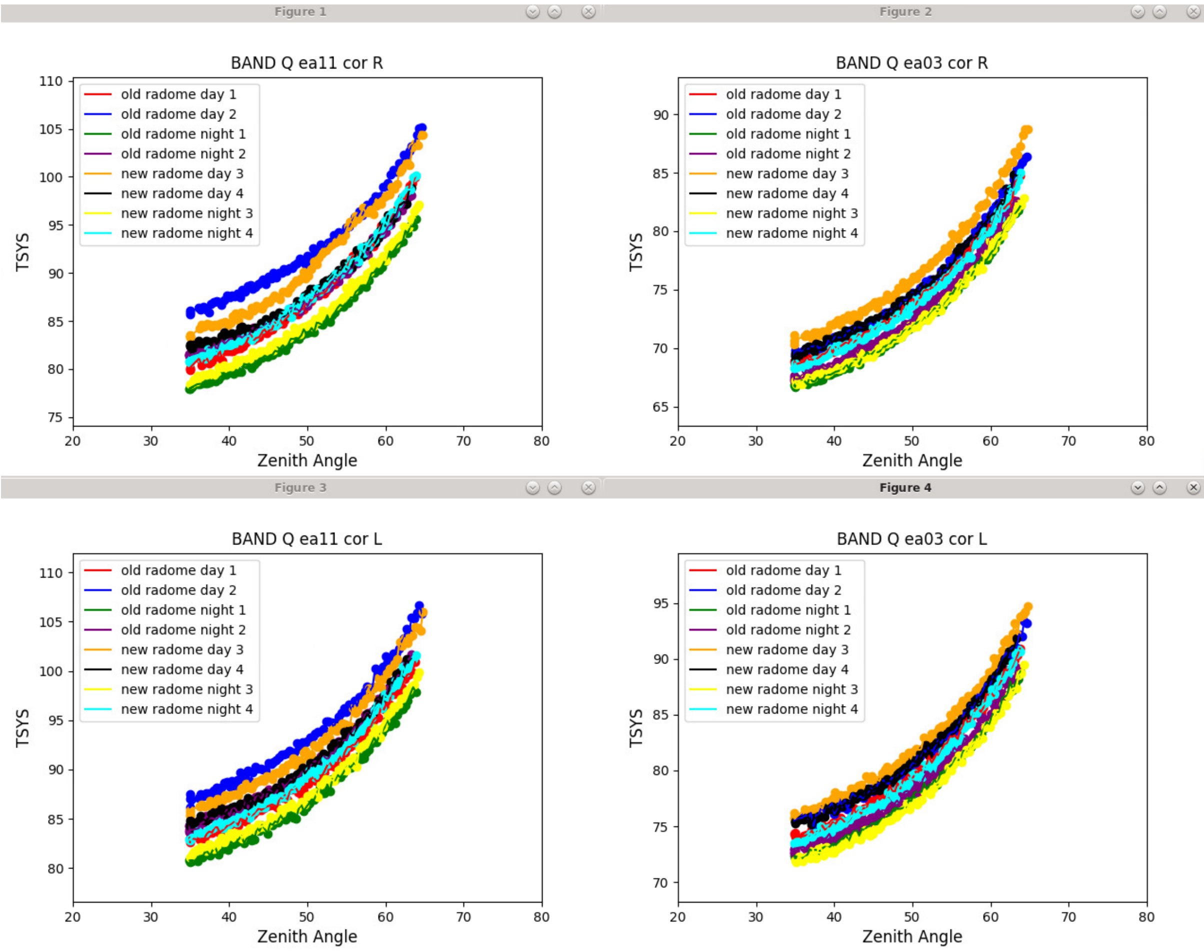

Figure 27: Tipping curves at Q-band. Comparing antenna ea11 and ea03, in both R and L. There are minor differences between the days, but no overall trend in direction of the observation with the new radome material, and nothing that was not seen in antenna ea03. We concluded that no differences could be attributed to the new radome material.

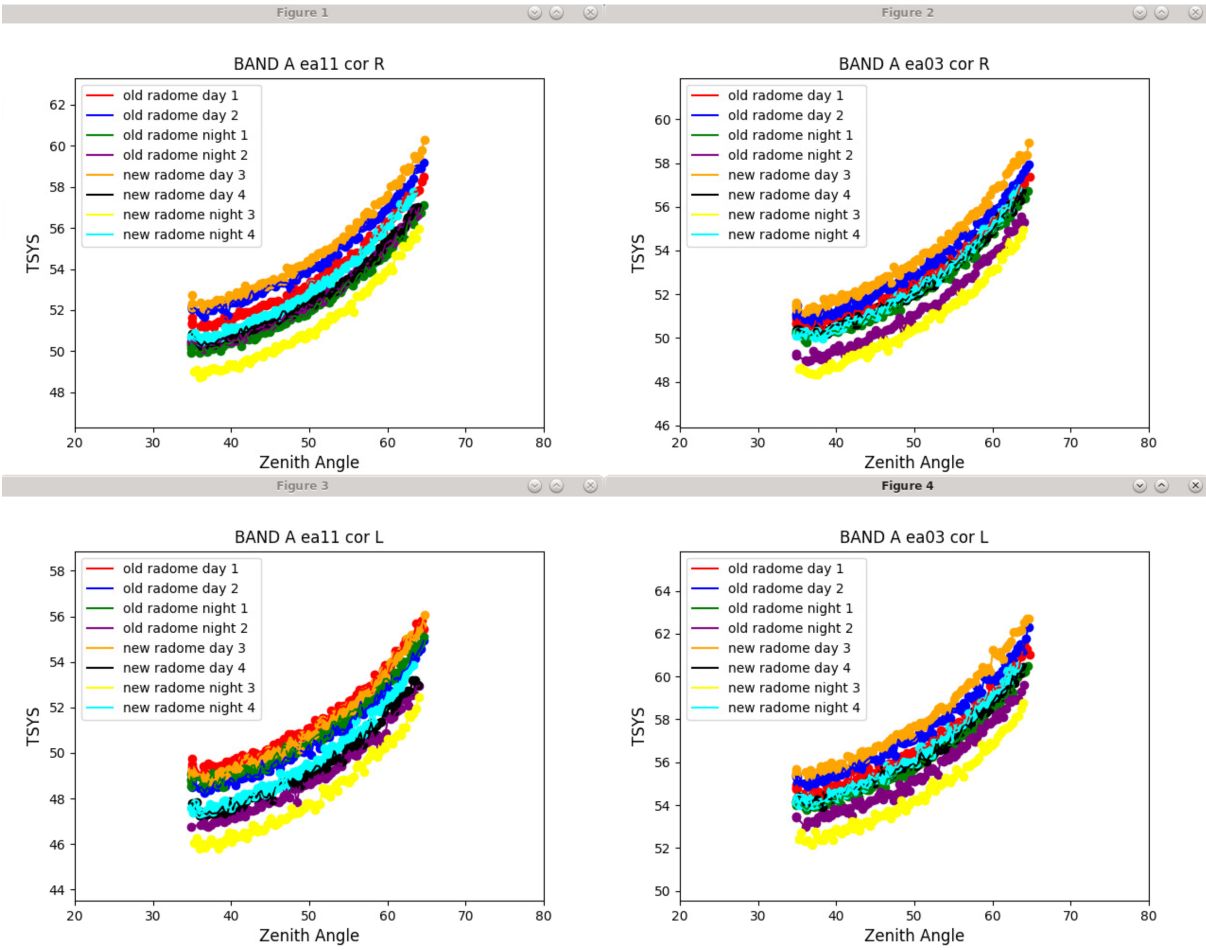

Figure 28: Tipping curves at Ka-band. Comparing antenna ea11 and ea03, in both R and L. There are minor differences between the days, but no overall trend in direction of the observation with the new radome material, and nothing that was not seen in antenna ea03. We concluded that no differences could be attributed to the new radome material.

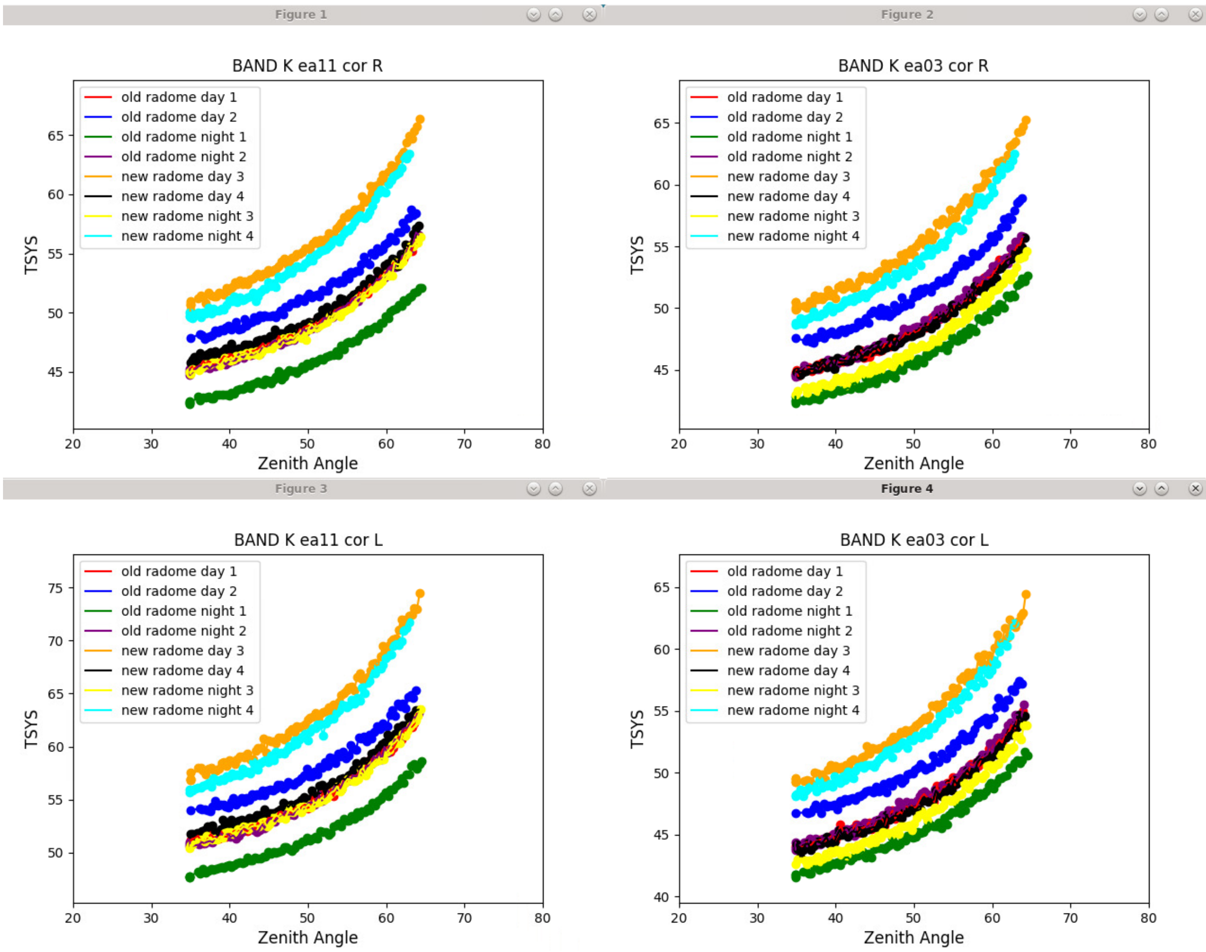

Figure 29: Tipping curves at K-band. Comparing antenna ea11 and ea03, in both R and L. There are minor differences between the days, but no overall trend in direction of the observation with the new radome material, and nothing that was not seen in antenna ea03. We concluded that no differences could be attributed to the new radome material.

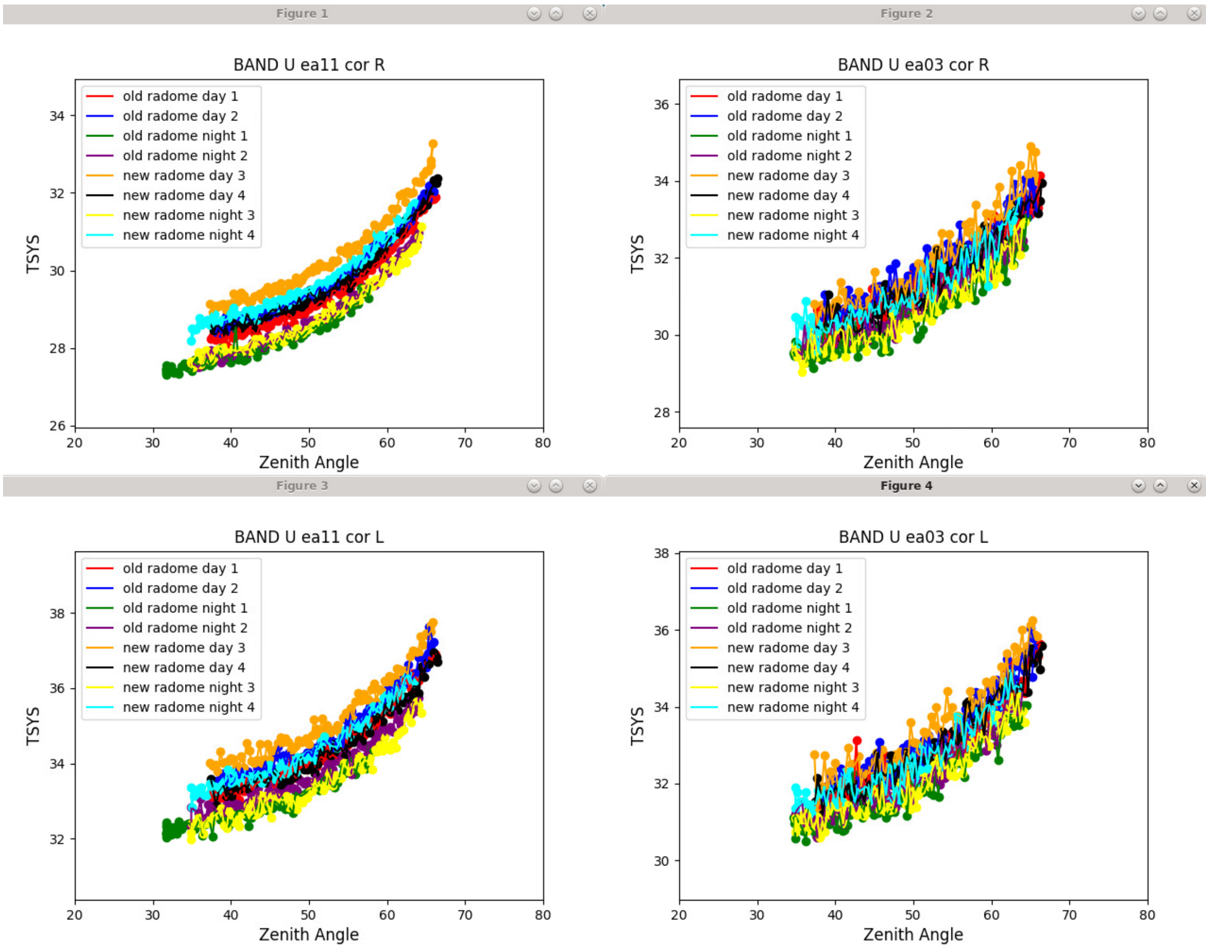

Figure 30: Tipping curves at Ku-band. Comparing antenna ea11 and ea03, in both R and L. There are minor differences between the days, but no overall trend in direction of the observation with the new radome material, and nothing that was not seen in antenna ea03. Due to many reasons, like spillover, RFI, and noise, we do not usually fit tipping curves at low frequencies. So our intent here is only to show the Tsys variability, no matter the opacity determination. We concluded that no differences could be attributed to the new radome material.

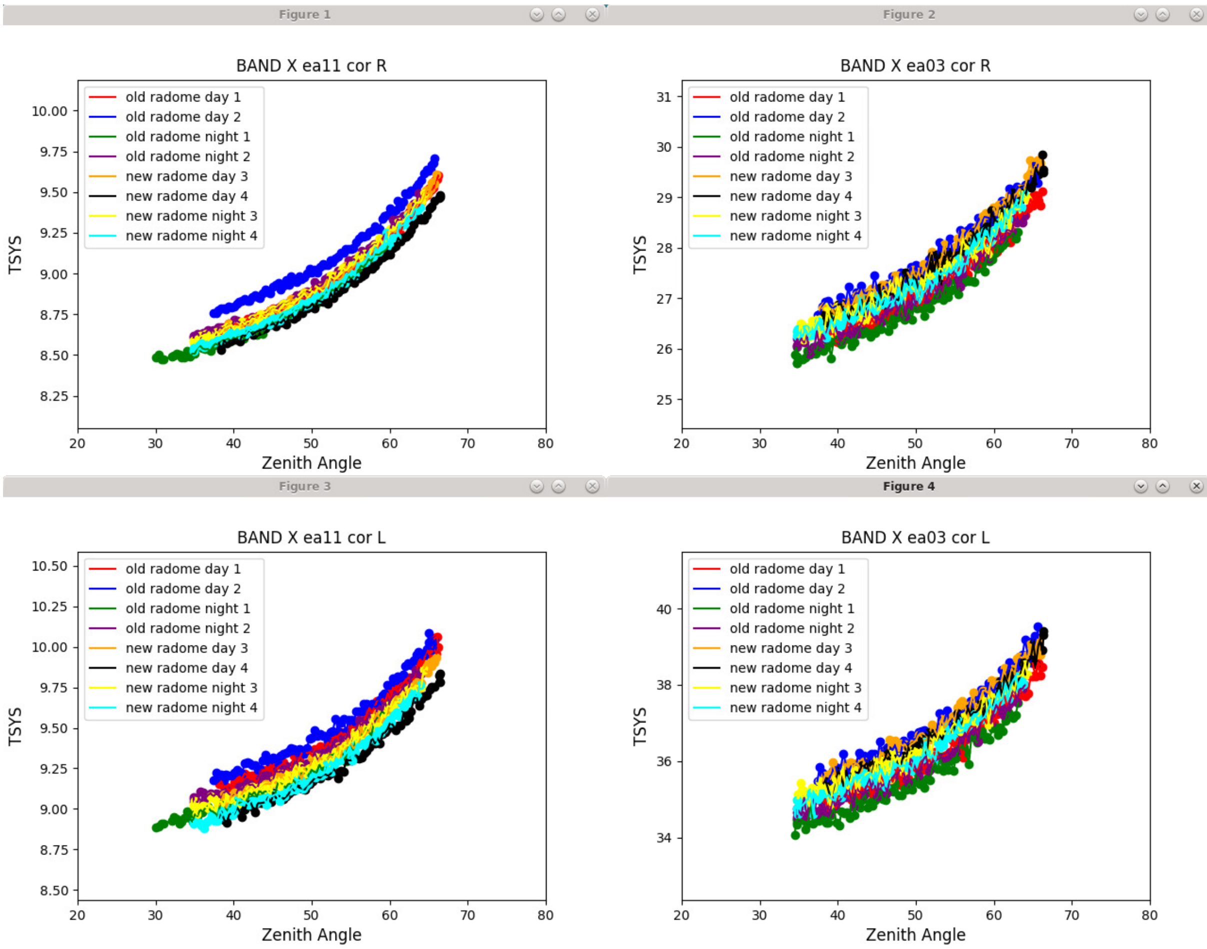

Figure 31: Tipping curves at X-band. Comparing antenna ea11 and ea03, in both R and L. There are minor differences between the days, but no overall trend in direction of the observation with the new radome material, and nothing that was not seen in antenna ea03. Due to many reasons, like spillover, RFI, and noise, we do not usually fit tipping curves at low frequencies. So our intent here is only to show the Tsys variability, no matter the opacity determination. We concluded that no differences could be attributed to the new radome material.

4.4 Cross-calibration

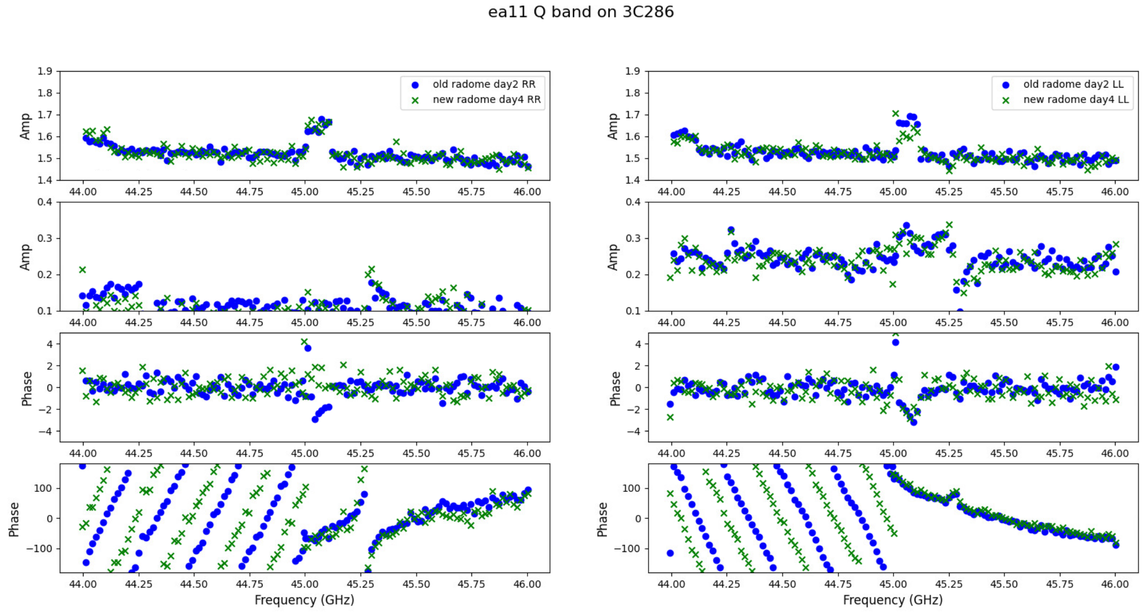

Figure 32. 3C286 observations at Q-band. In this plot, we used the calibration table obtained from the observations with the old radome material, and we have applied to the observations with the new radome, to verify any eventual changes.We show only the best day before and after. All changes seen in ea11 are also seen in ea03 (Figure 33), like the phase delay on RL and LR. We concluded that no differences could be attributed to the new radome material.

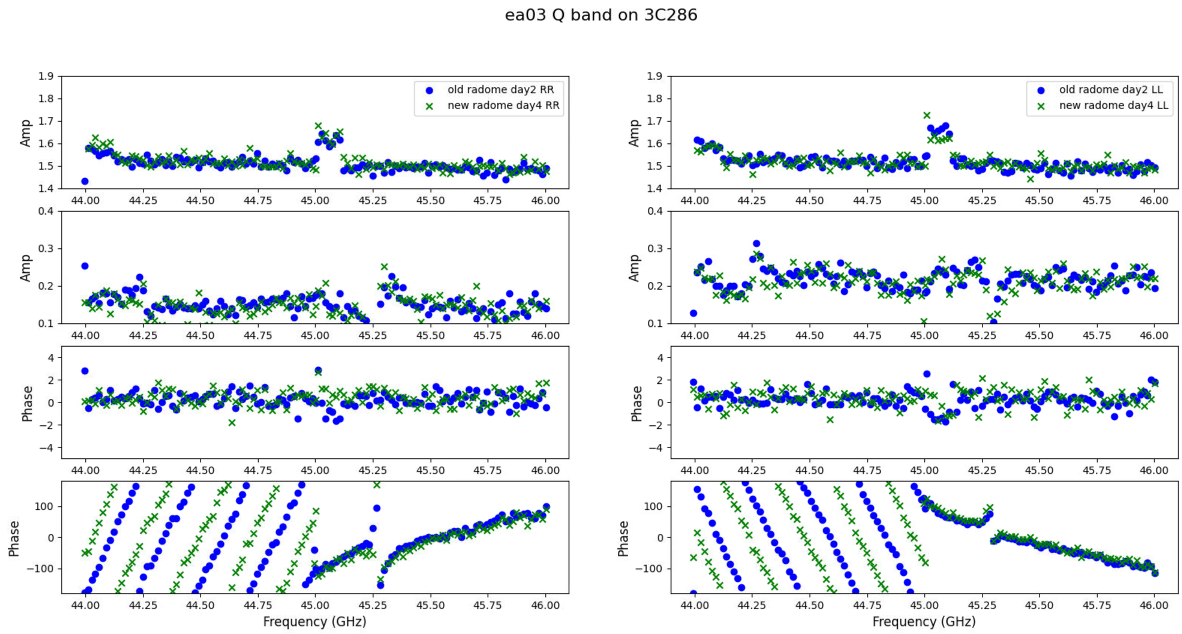

Figure 33. 3C286 observations at Q-band. In this plot, we used the calibration table obtained from the observations with the old radome material, and we have applied to the observations with the new radome, to verify any eventual changes.We show only the best day before and after. All changes seen in ea11 (Figure 32) are also seen in ea03, like the phase delay on RL and LR. We concluded that no differences could be attributed to the new radome material.

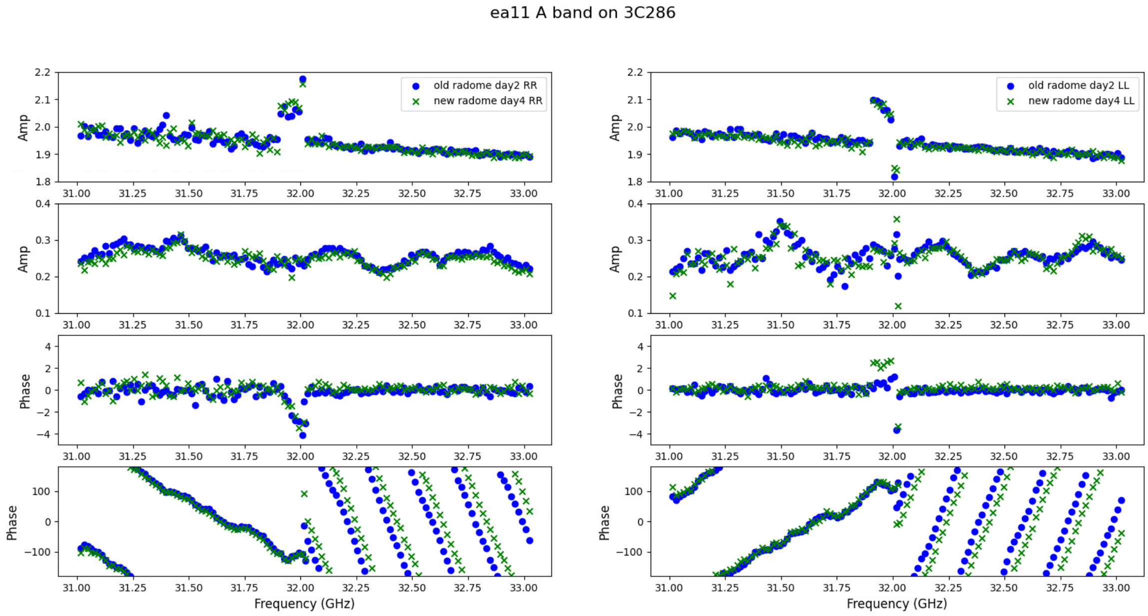

Figure 34. 3C286 observations at Ka-band. In this plot, we used the calibration table obtained from the observations with the old radome material, and we have applied to the observations with the new radome, to verify any eventual changes.We show only the best day before and after. All changes seen in ea11 are also seen in ea03 (Figure 35), like the phase delay on RL and LR. We concluded that no differences could be attributed to the new radome material.

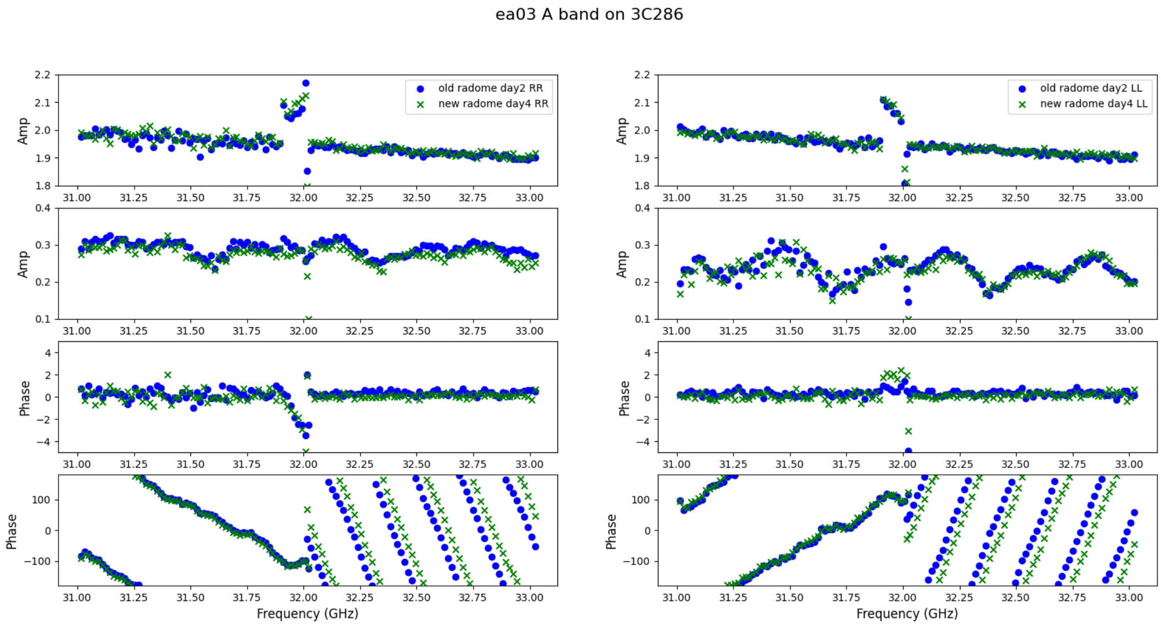

Figure 35. 3C286 observations at Ka-band. In this plot, we used the calibration table obtained from the observations with the old radome material, and we have applied to the observations with the new radome, to verify any eventual changes.We show only the best day before and after. All changes seen in ea11 (Figure 34) are also seen in ea03, like the phase delay on RL and LR. We concluded that no differences could be attributed to the new radome material.

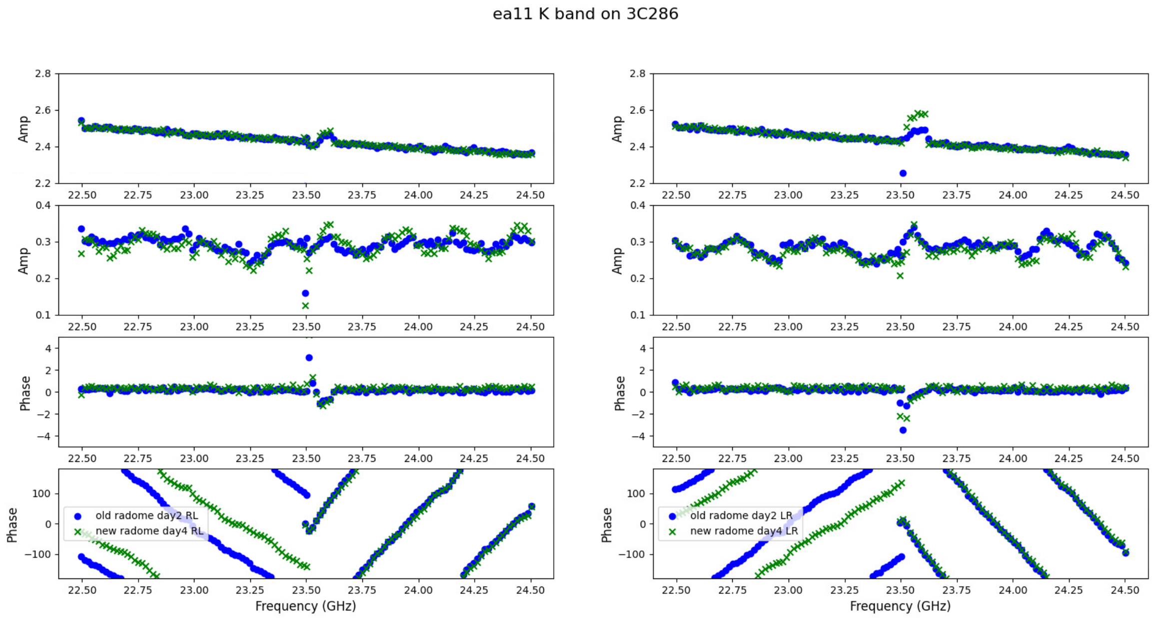

Figure 36. 3C286 observations at K-band. In this plot, we used the calibration table obtained from the observations with the old radome material, and we have applied to the observations with the new radome, to verify any eventual changes.We show only the best day before and after. All changes seen in ea11 are also seen in ea03 (Figure 37), like the phase delay on RL and LR. We concluded that no differences could be attributed to the new radome material.

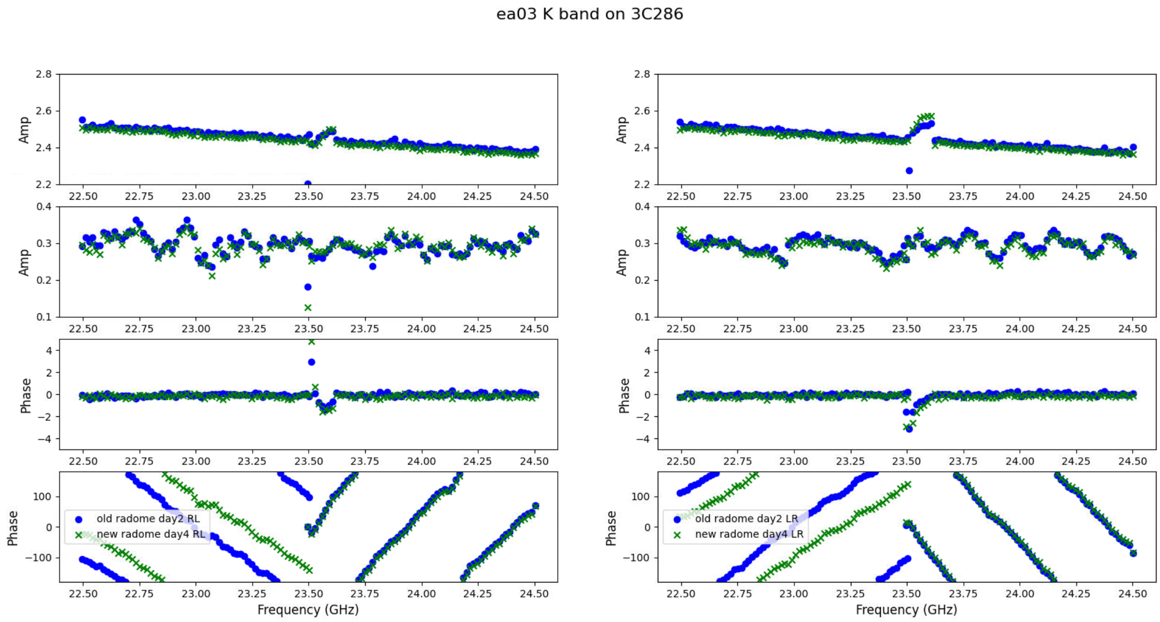

Figure 37. 3C286 observations at K-band. In this plot, we used the calibration table obtained from the observations with the old radome material, and we have applied to the observations with the new radome, to verify any eventual changes.We show only the best day before and after. All changes seen in ea11(Figure 36) are also seen in ea03, like the phase delay on RL and LR. We concluded that no differences could be attributed to the new radome material.

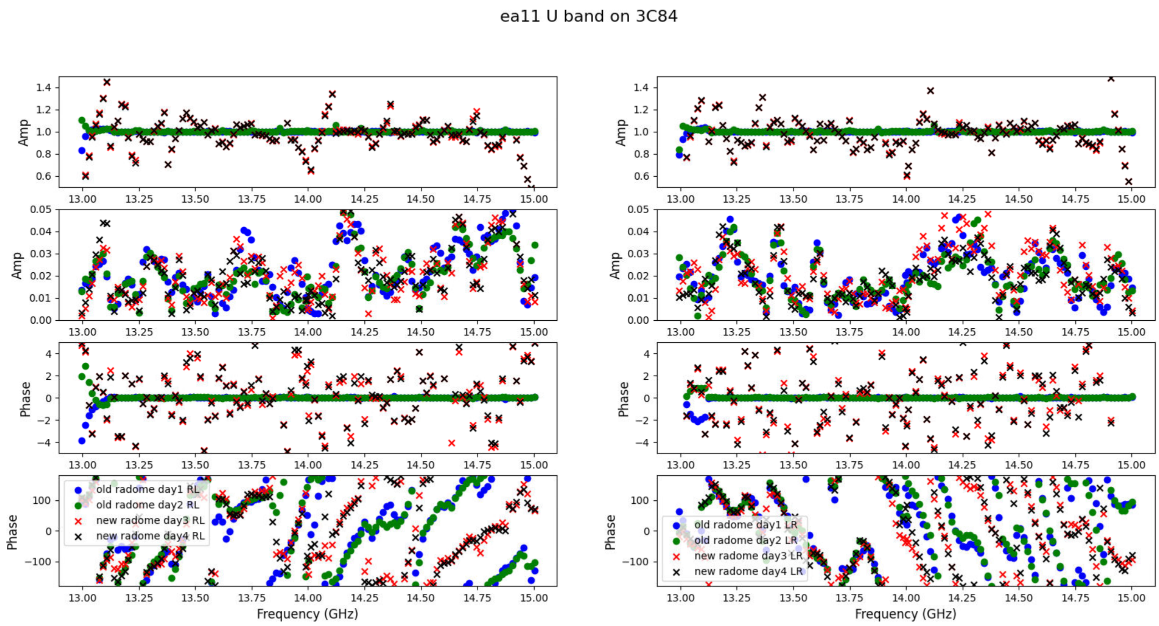

Figure 38. 3C84 observations at Ku-band. In this plot, we used the calibration table obtained from the observations with the old radome material, and we have applied to the observations with the new radome, to verify any eventual changes. The signature of the bandpass solution in day 3 and day 4 is clear, but it is also presented in ea03 (Figure 39). We concluded that no differences could be attributed to the new radome material.

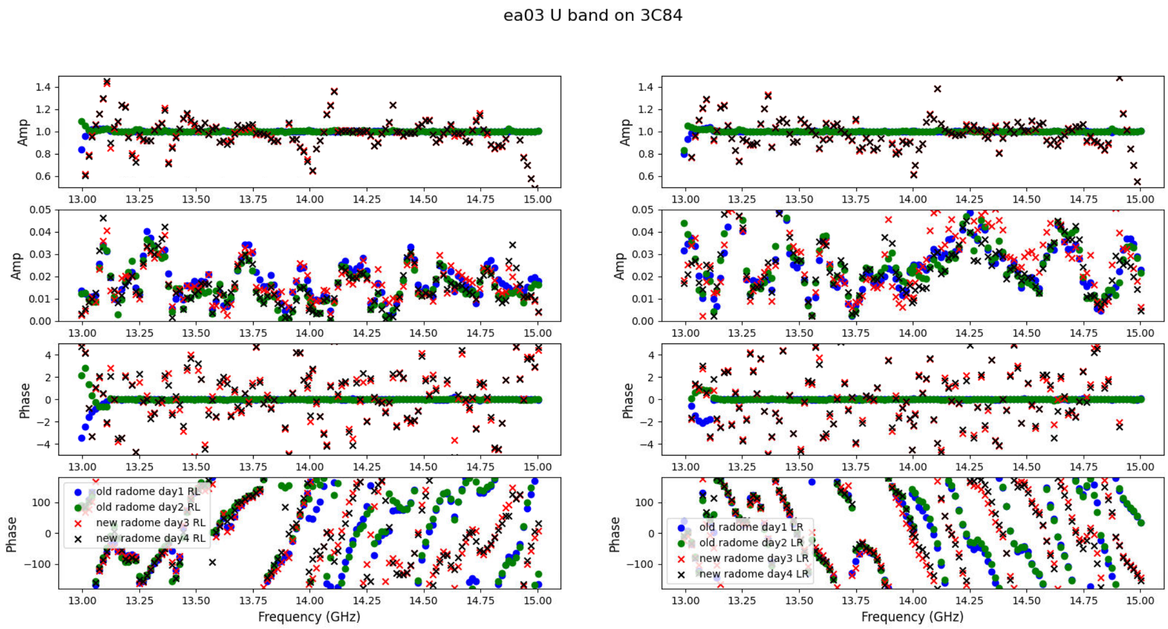

Figure 39. 3C84 observations at Ku-band. In this plot, we used the calibration table obtained from the observations with the old radome material, and we have applied to the observations with the new radome, to verify any eventual changes. The signature of the bandpass solution in day 3 and day 4 is clear, but it is also presented in ea03 (see Figure 38 for ea11). We concluded that no differences could be attributed to the new radome material.

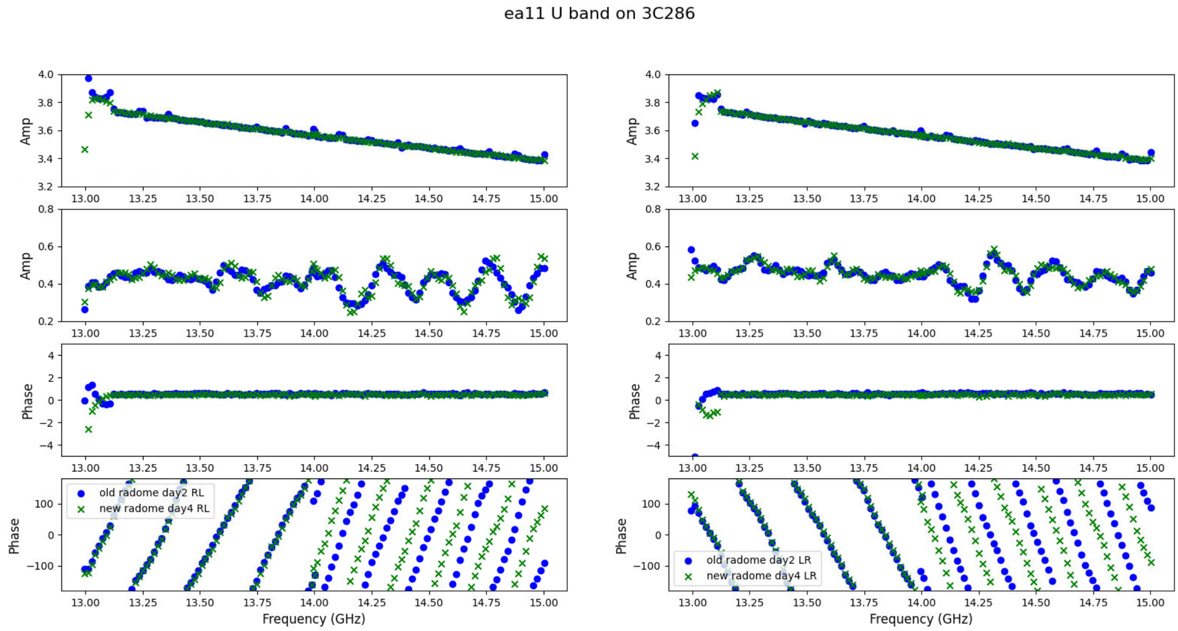

Figure 40. 3C286 observations at Ku-band. In this plot, we used the calibration table obtained from the observations with the old radome material, and we have applied to the observations with the new radome, to verify any eventual changes.We show only the best day before and after. All changes seen in ea11 are also seen in ea03 (Figure 41), like the phase delay on RL and LR. We concluded that no differences could be attributed to the new radome material.

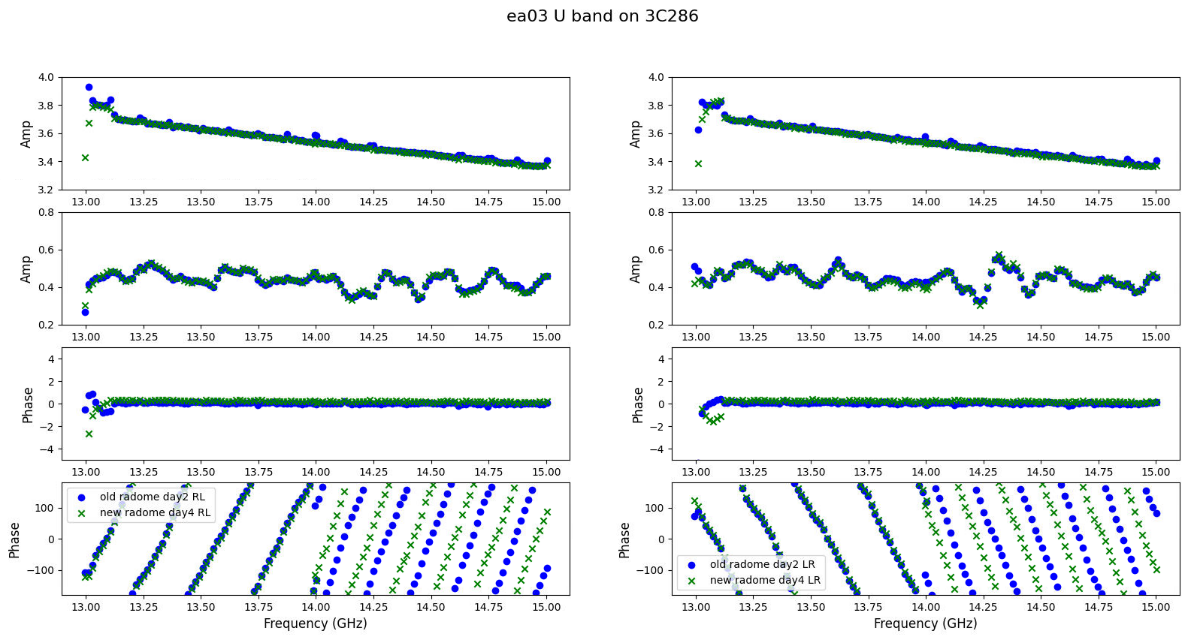

Figure 41. 3C286 observations at Ku-band. In this plot, we used the calibration table obtained from the observations with the old radome material, and we have applied to the observations with the new radome, to verify any eventual changes.We show only the best day before and after. All changes seen in ea11 (Figure 40) are also seen in ea03, like the phase delay on RL and LR. We concluded that no differences could be attributed to the new radome material.

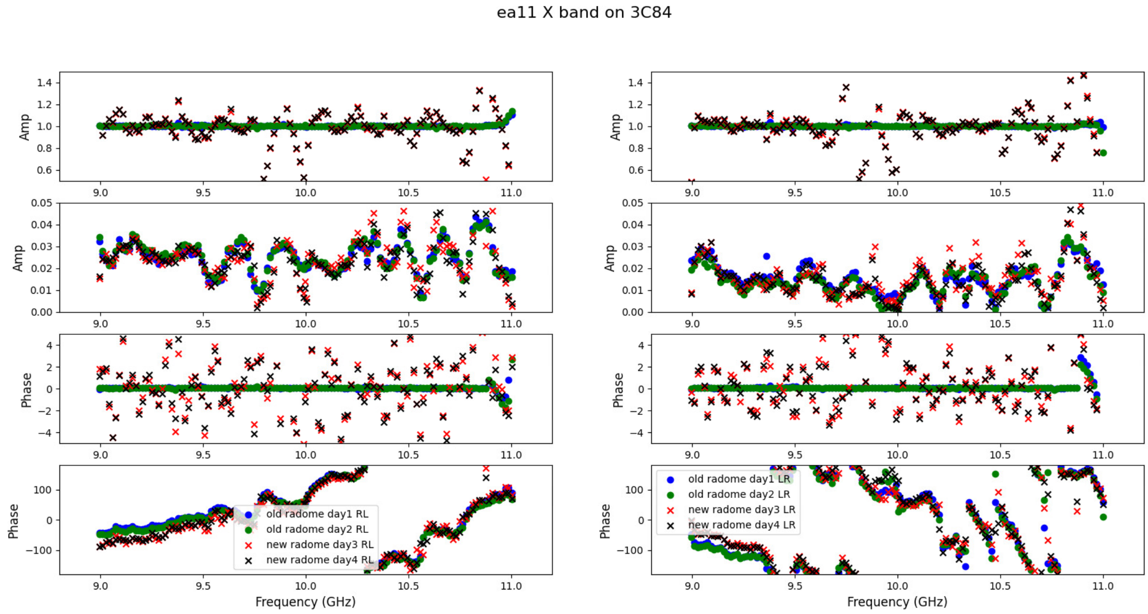

Figure 42. 3C84 observations at X-band. In this plot, we used the calibration table obtained from the observations with the old radome material, and we have applied to the observations with the new radome, to verify any eventual changes. The signature of the bandpass solution in day 3 and day 4 is clear, as we saw in Ku-band (figures 38 and 39) and it is also presented in ea03 (Figure 43). We concluded that no differences could be attributed to the new radome material.

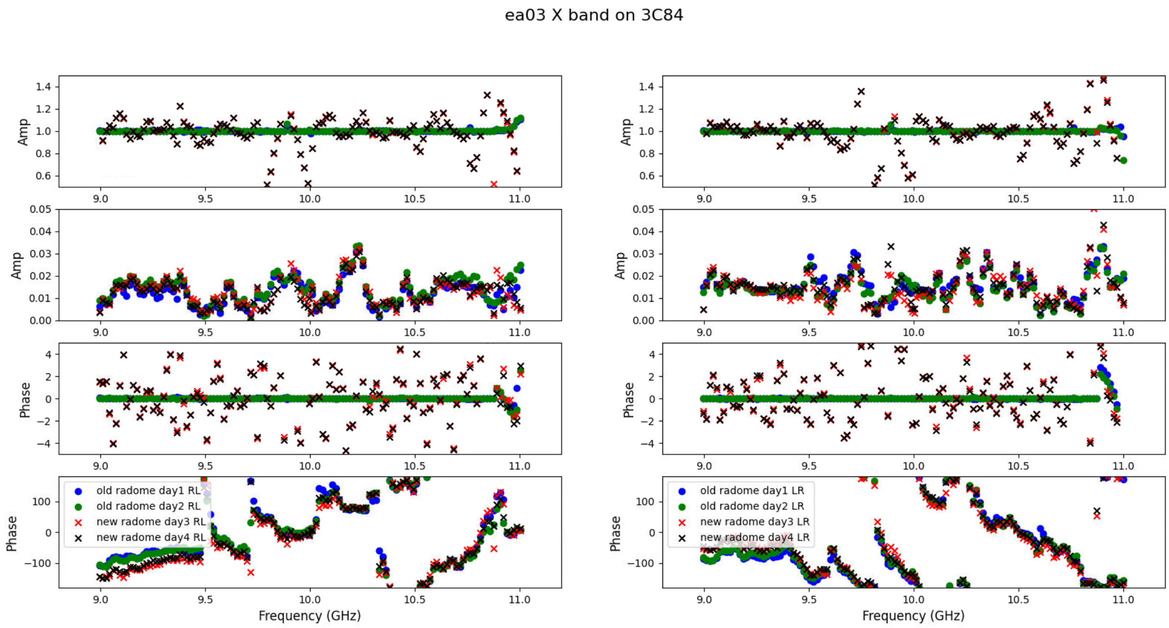

Figure 43. 3C84 observations at X-band. In this plot, we used the calibration table obtained from the observations with the old radome material, and we have applied to the observations with the new radome, to verify any eventual changes. The signature of the bandpass solution in day 3 and day 4 is clear, as we saw in Ku-band (figures 38 and 39) and it is also presented in ea03 (ea 11 in Figure 42). We concluded that no differences could be attributed to the new radome material.

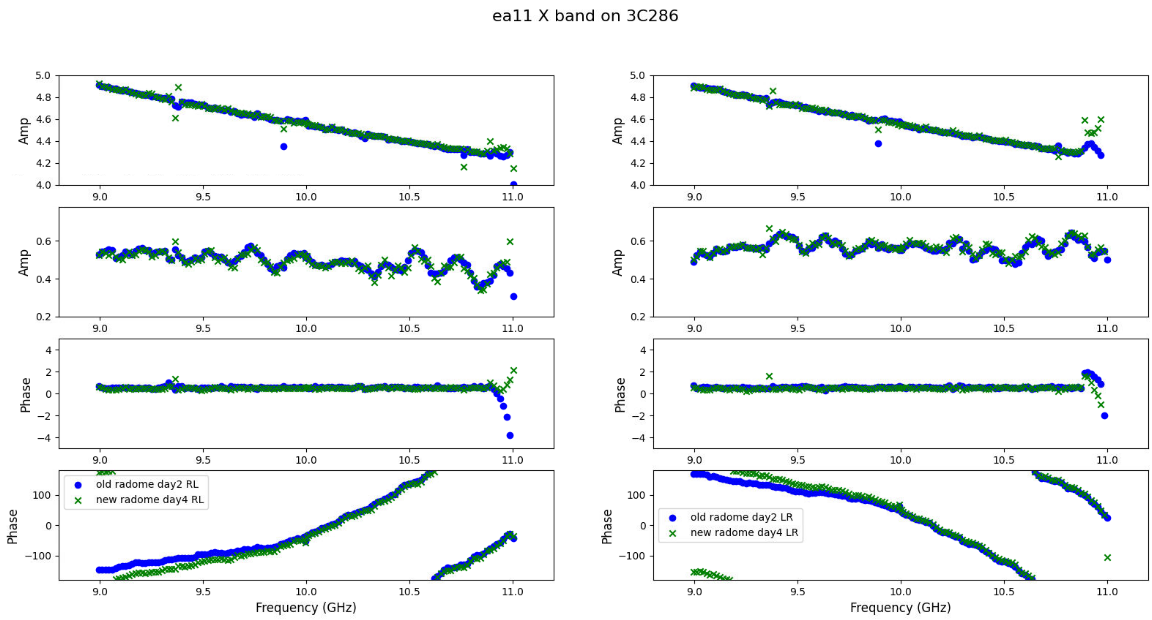

Figure 44. 3C286 observations at X-band. In this plot, we used the calibration table obtained from the observations with the old radome material, and we have applied to the observations with the new radome, to verify any eventual changes.We show only the best day before and after. All changes seen in ea11 are also seen in ea03 (Figure 45), like the phase delay on RL and LR. We concluded that no differences could be attributed to the new radome material.

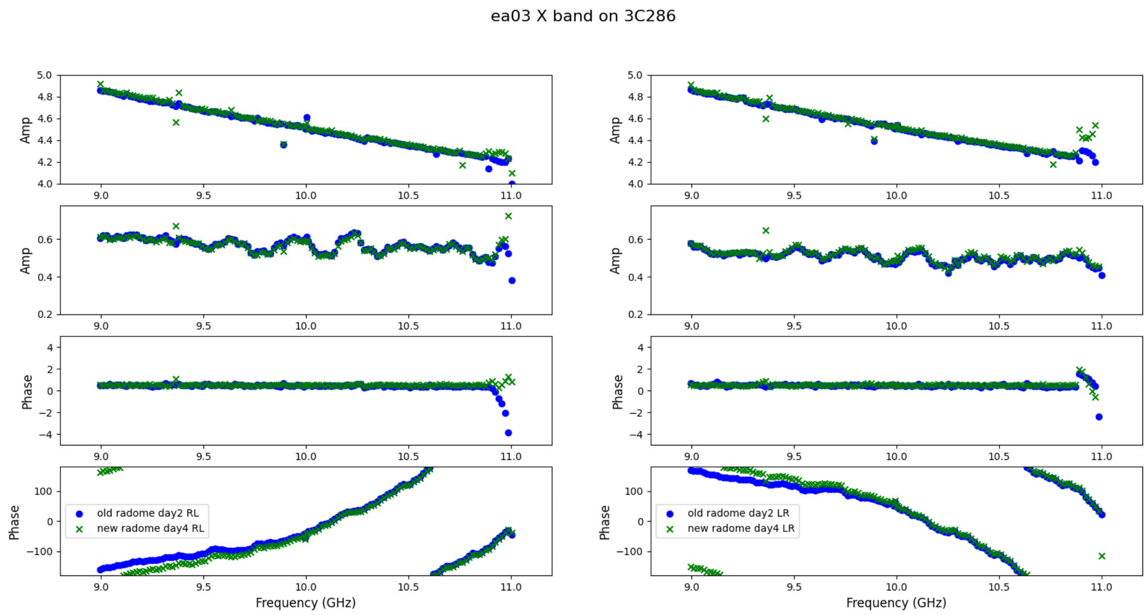

Figure 45. 3C286 observations at X-band. In this plot, we used the calibration table obtained from the observations with the old radome material, and we have applied to the observations with the new radome, to verify any eventual changes.We show only the best day before and after. All changes seen in ea11 (Figure 44) are also seen in ea03, like the phase delay on RL and LR. We concluded that no differences could be attributed to the new radome material.

5. Conclusions

We show several plots comparing data of four observations performed with the old radome material and the other four performed with the new radome material. We see no major differences. Minor changes in Tsys are also seen in antenna ea03, the closest antenna to ea11. When needed, we also show data of ea28, used as a reference antenna, and ea10, another antenna close but in the east arm. We conclude that there are no significant differences in the signal due to the new radome material.

Appendix A

Table A.1 shows the file names of each observation presented in the archive using source 3C84, while table A.2 shows observations of the source 3C286. In both cases, the two first observations were with the old radome while the two last with the new material.

Table A.1: File names, days and sizes for 3C84 observations

Day	File Name	OBS Start	OBS End	Size (GB)
4/9	THIG0007_sb41670604_1_1.59678.022201851854	00:31:58	01:39:45	14.210
4/10	THIG0007_sb41670604_1_1_000.59678.98967113426	23:45:08*	00:52:54	14.238
4/15	THIG0007.sb41670604.eb41768976.59683.9725606713	23:23:01*	00:30:48	15.308
4/16	THIG0007.sb41670604.eb41772650.59685.02146570601	00:30:55	01:38:41	15.322

*started on the day before.

Table A.2: File names, days and sizes for 3C286 observations

Day	File Name	OBS Start	OBS End	Size (GB)
4/9	THIG0007_sb41755714_1_1.59678.171051296296	04:06:19	05:22:04	16.066
4/10	THIG0007_sb41755714_1_1_000.59679.16467967593	03:57:08	05:12:53	16.078
4/14	THIG0007.sb41755714.eb41766924.59683.09901900463	02:22:35	03:38:18	17.308
4/15	THIG0007.sb41755714.eb41768982.59684.111520266204	02:40:35	03:56:17	17.296